

The FAST Galactic Plane Pulsar Snapshot survey: VIII. 112 binary pulsars

P. F. WANG,^{1,2,3} J. L. HAN,^{1,2,3} Z. L. YANG,^{1,2} T. WANG,¹ C. WANG,^{1,2,3} W. Q. SU,^{1,2} J. XU,^{1,3} D. J. ZHOU,¹ YI YAN,¹
W. C. JING,^{1,2} N. N. CAI,¹ J. P. YUAN,⁴ R. X. XU,^{5,6} H. G. WANG,⁷ AND X. P. YOU⁸

¹National Astronomical Observatories, Chinese Academy of Sciences, Jia-20 Datun Road, ChaoYang District, Beijing 100012, China

²School of Astronomy and Space Science, University of Chinese Academy of Sciences, Beijing 100049, China

³Key Laboratory of Radio Astronomy and Technology, Chinese Academy of Sciences, Beijing 100101, China

⁴Xinjiang Astronomical Observatory, Chinese Academy of Sciences, 150 Science 1-street, Urumqi 830011, China

⁵Department of Astronomy, Peking University, Beijing 100871, China

⁶Kavli Institute for Astronomy and Astrophysics, Peking University, Beijing 100871, China

⁷Department of Astronomy, School of Physics and Materials Science, Guangzhou University, Guangzhou 510006, China

⁸School of Physical Science and Technology, Southwest University, Chongqing 400715, China

ABSTRACT

Finding pulsars in binaries are important for measurements of the masses of neutron stars, for tests of gravity theories, and for studies of star evolution. We are carrying out the Galactic Plane Pulsar Snapshot survey (GPPS) by using the the Five-hundred-meter Aperture Spherical radio Telescope (FAST). Here we present the Keplerian parameters for 112 newly discovered pulsars in the FAST GPPS survey, and obtain timing solutions for 27 pulsars. Companions of these pulsars are He white dwarfs, CO/ONe white dwarfs, neutron stars, main sequence stars and ultra light objects or even planets. Our observations uncover eclipses of 8 binary systems. The optical counterpart for the companion of PSR J1908+1036 is identified. The Post Keplerian parameter $\dot{\omega}$ for the double neutron star systems PSR J0528+3529 and J1844-0128 have been determined, with which the total masses of the binary systems are determined.

Keywords: pulsars: general

1. INTRODUCTION

Pulsars are rapidly rotating neutron stars with spin periods ranging from about 1.39 millisecond to several tens of seconds (Manchester et al. 2005, see updated catalogue 2.4.0¹). They are formed through supernova explosion of massive stars ($8-25M_{\odot}$) at the end of stellar evolution or accretion induced collapse of massive white dwarfs (WDs). Pulsars serve as important laboratories for studying fundamental physics due to their super high density, extremely strong magnetic field and gravitational field. They have been employed to detect low-frequency gravitational waves through pulsar timing arrays (e.g. Lentati et al. 2015; Alam et al. 2021; Reardon et al. 2021; Xu et al. 2023), test the theory of gravity (e.g. Freire et al. 2012), constrain the equation of state (EOS) of neutron star by mass measurement (e.g. Demorest et al. 2010; Antoniadis et al. 2013; Özel & Freire 2016), and construct pulsar-based time-scale (Hobbs et al. 2020).

Among 3724 known pulsars (Manchester et al. 2005), 421 pulsars are in binary systems. Most of the pulsars in binary systems are millisecond pulsars (MSPs) with spin periods

of $P \leq 30$ ms and spin-down rate $\dot{P} \leq 10^{-17}$. These binary MSPs are generally believed to be spun up by accreting material from their companion (e.g. Alpar et al. 1982; Bhattacharya & van den Heuvel 1991), so they are called as “recycled pulsars”. During recycling, the magnetic field strength of pulsars are reduced and their orbits are circularized. Companions of these binary pulsars can be neutron stars (NS), white dwarfs (WD), main sequence stars (MS), ultra-light companion (UL) such as brown dwarf or white dwarf remnant or planet with mass $m_c \leq 0.1M_{\odot}$. The spin periods P , pulsar ellipses, orbital periods P_b , orbital eccentricity e and median companion masses $m_{c,med}$ derived from mass functions can be used as criteria to classify companion types, see Table 1. For example, some MSPs in compact orbits ($P_b < 1$ day) with a low-mass non- or semi-degenerate companion are “spiders”, in which the pulsar winds are evaporating the companion. Many of them show the eclipses of pulsar signals. They are further divided into “black-widows” if the companion mass is less than $\sim 0.1M_{\odot}$ (their companions are “UL”) or “redbacks” if the mass is greater than $\sim 0.1M_{\odot}$ (their companions are probably evolved MSs) (Roberts 2013; Chen et al. 2013).

Binary systems have diverse formation history. It is generally accepted that double neutron star systems originate from high-mass X-ray binaries (HMXB) via a common envelope

Corresponding to: hjl@nao.cas.cn; pfwang@nao.cas.cn

¹ <https://www.atnf.csiro.au/people/pulsar/psrcat/>

Table 1. Parameter ranges for known binary pulsars with various companion types in the Galactic field and the classification criteria

Companion type	P (ms)	P_b (days)	$m_{c,med}$ (M_\odot)	e	Coarse classification Criteria
He-WD	[1.74, 834.84]	[0.10, 944.64]	[0.07, 0.48]	$[1.2 \times 10^{-7}, 0.14]$	$m_{c,med} > 0.08M_\odot$ & $P < 10\text{ms}$ & [$(m_{c,med} < 0.23M_\odot$ & $P_b < 5\text{d})$ or $(m_{c,med} < 0.356M_\odot$ & $5\text{d} < P_b < 100\text{d})$ or $(m_{c,med} < 0.5M_\odot$ & $P_b > 100\text{d})$]
CO/ONe-WD	[2.91, 1066.37]	[0.19, 95.26 [†]]	[0.33 [†] , 1.58]	$[6.9 \times 10^{-7}, 0.66]$	$m_{c,med} > 0.356M_\odot$ & $P_b < 100\text{d}$ & $e < 0.05$
MS star (unevolved)	[47.76 [‡] , 763.93]	[95.17, 16800]	[1.08, 18.50]	[0.08, 0.96]	$m_{c,med} > 1.0M_\odot$ & $P_b > 80\text{d}$ & $e > 0.05$ & $P > 30\text{ms}$
MS star (evolved)	[1.61, 14.25]	[0.08, 1.1*]	[0.11, 0.52]	$[4.2 \times 10^{-6}, 2.1 \times 10^{-4}]$	$0.1M_\odot < m_{c,med} < 0.52M_\odot$ & $P_b < 1.1\text{d}$ & $e < 0.001$ & $P < 30\text{ms}$ & Eclipse
Neutron star (NS)	[16.96 2773.46]	[0.078, 45.06]	[0.76, 1.74]	[0.06, 0.83]	$m_{c,med} > 0.76M_\odot$ & $P_b < 80\text{d}$ & $e > 0.05$
Ultra light object (UL)	[1.41, 520.95]	[0.06, 10.59]	[0.0009, 0.097]	$[2.6 \times 10^{-6}, 4.5 \times 10^{-3}]$	$m_{c,med} < 0.08M_\odot$

NOTE—[†]: J0823+0159 has a CO WD companion with an orbital period of 1232.4 days and a median mass of $0.226M_\odot$ (Koester & Reimers 2000), [‡]: J1903+0327 has a MS companion, a spin period of 2.150ms and an orbital period of 95.2 days (Freire et al. 2011), *: J1417–4402 has a red-giant companion with an orbital period of 5.4 days (Strader et al. 2015)

(CE) and spiral-in process (e.g. Tauris & van den Heuvel 2006). Pulsars with CO/ONe white dwarf companions originate from intermediate-mass X-ray binaries (IMXBs, e.g. Tauris et al. 2012), and the ones with He white dwarf companions originate from low-mass X-ray binaries (LMXBs, e.g. Pylyser & Savonije 1988; Istrate et al. 2014). The final orbital configuration and stellar masses are diverse, depending on the companion mass and metallicity, the initial orbital separation as well as the evolution stage of the donor star when Roche-Lobe Overflow (RLO) initiates, for example, the Case A RLO on the main sequence stage, the Case B RLO at the red giant branch (RGB) stage with hydrogen shell burning, the Case C RLO for the asymptotic giant branch (AGB) stage with helium shell burning (e.g. Tauris & van den Heuvel 2023). Hence, the spin period, period derivative, orbital period, orbit eccentricity, and masses of pulsar and its companion are important fossil records for the original binary evolution (e.g. Corbet 1984; Phinney 1992). Based on observations of binary pulsars, the evolution theories of stellar binaries have been developed and examined (e.g. Tauris et al. 2012; Istrate et al. 2014; Chen et al. 2021).

Binary systems with compact orbits generally exhibit a number of relativistic effects which can be quantified by Post-Keplerian (PK) parameters. With two PK parameters, masses of the pulsar and the companion as well as the inclination angle of the orbit can be determined by resorting to a theory of gravity, e.g. General Relativity (GR) (e.g. Özel & Freire 2016). By combing these precisely measured pulsar masses, underlying distribution of neutron star masses can be determined (Antoniadis et al. 2016). Masses of the most massive neutron stars pose important constraints on the equation of state (EOS) of neutron stars, e.g. PSRs J0348+0432, J0740+6620 and J1614–2230 (e.g. Demorest et al. 2010; Antoniadis et al. 2013; Özel & Freire 2016). The so measured companion masses can be employed to test the theories of binary evolution (Phinney & Kulkarni 1994; Tauris &

Savonije 1999). Combination of more than two PK parameters allows for the tests of GR and other theory of gravity in the strong-field regime with high precision (Weisberg & Taylor 1984; Kramer et al. 2006). The violation of strong equivalence principle can also be tested by constraining the universality of free fall or gravitational dipole radiation (Freire et al. 2012; Voisin et al. 2020). Moreover, relativistic deformation of the orbit (Weisberg & Huang 2016; Cameron et al. 2018) and relativistic spin-orbit coupling or named as Lense-Thirring process (Cameron et al. 2018; Hu et al. 2020; Venkatraman Krishnan et al. 2020) can also be detected from the change of orbital inclination.

Finding and precisely timing new binary systems, especially those with compact orbits, exceptional orbital configurations or the most massive pulsars, will improve the existing tests of gravity, the constraints of EOS and and the understanding the evolution channels of stellar binaries. There have been many efforts devoted to precise measurements of the binary nature of the systems (e.g. Deneva et al. 2021; Kramer et al. 2021; Miao et al. 2023), and most of them are follow-up observations of new pulsars discovered in large pulsar survey projects.

We are carrying out the Galactic Plane Pulsar Snapshot (GPPS) survey (Han et al. 2021) by using the the Five-hundred-meter Aperture Spherical radio Telescope (FAST, Nan 2006; Nan et al. 2011), with a goal to discover pulsars within the Galactic latitude of $\pm 10^\circ$ of the FAST visible sky area. Up to now, we have discovered 751 pulsars² (Han et al. 2024). Among them about 160 pulsars show binary features, such as prominent acceleration in the discovery diagram or a significant variation of barycentric periods in the confirmation observation. We ascertain their binary nature with a few follow-up observations, and get the orbital parameters deter-

² <http://zmtt.bao.ac.cn/GPPS/GPPSnewPSR.html>

Table 2. FAST projects for collecting data for binary pulsar timing in this paper.

Project ID	PI	Observation hours
ZD2020_2	J.L. Han	350+
ZD2021_2	J.L. Han	350+
ZD2022_2	J.L. Han	350+
ZD2023_2	J.L. Han	350+
ZD2024_2	J.L. Han	350+
PT2020_0136	P.F. Wang	30.0
PT2021_0037	T. Wang	42.0
PT2021_0126	P.F. Wang	40.0
PT2022_0047	W.Q. Su	70.0
PT2022_0158	Z.L. Yang	20.0
PT2022_0159	T. Wang	20.0
PT2022_0174	P.F. Wang	20.0
PT2022_0178	Z.L. Yang	15.0
PT2023_0084	Z.L. Yang	18.9
PT2023_0085	P.F. Wang	19.5
PT2023_0143	Z.L. Yang	15.8
PT2023_0162	W.Q. Su	11.5
PT2023_0190	P.F. Wang	7.6
PT2023_0193	Z.L. Yang	11.5
PT2023_0195	Z.L. Yang	11.2
PT2024_0007	P.F. Wang	23.3
PT2024_0020	Z.L. Yang	31.9
PT2024_0026	P.F. Wang	25.0
PT2024_0200	Z.L. Yang	13.1
PT2024_0224	Z.L. Yang	5.6
PT2024_0231	Z.L. Yang	5.4

mined for about 3/4 of them. More follow-up observations of these binary pulsars have been done by several applied FAST projects, see Table 2. Combining all data, we get timing solutions for some of them (see Table 3) and Table A1 in appendix.. The first pulsar discovered by the GPPS survey, PSR J1901+0658 (gpps0001), is turned out to be a double neutron star system (Su et al. 2024). The 190th GPPS pulsar, PSR J1953+1844 (gpps0190), is in a binary with the shortest orbital period of only 53 minutes (Pan et al. 2023), probably a descendant of an ultracompact X-Ray binary (Yang et al. 2023). PSR J1928+1815 (gpps0121) is an eclipsed millisecond pulsar in a compact orbit with an orbital period of 3.6 hours, standing as evidence for the common envelope phase (Yang et al. 2024b). We get timing solution for 6 millisecond pulsars in compact orbits with massive white dwarf companions (Yang et al. 2024a). Here, we present the results for 112 new binary pulsars, as listed in Table 3. In Section 2, we briefly describe the FAST observations and data reduction procedures. The Keplerian solutions and timing solutions are presented in Section 3 together with companion classification. Conclusions and further discussion are given in Section 4.

2. FAST OBSERVATIONS AND DATA REDUCTION

All FAST Observations used in this paper (see Table 2) have been carried out by using the 19-beam L-band receiver. In the GPPS survey observations (ZD2020_2 to ZD2024_2), the snapshot observation mode has been used to cover a hexagonal sky area of 0.1575 square degrees by using 76

beams (see Fig. 4 in Han et al. 2021). The follow-up observations have been carried out by using the tracking mode and also the 19-beam L-band receiver, including these verification observations made by the ZD202x_2 or the targeted observations by other free-applied projects (PT202x_0vvv).

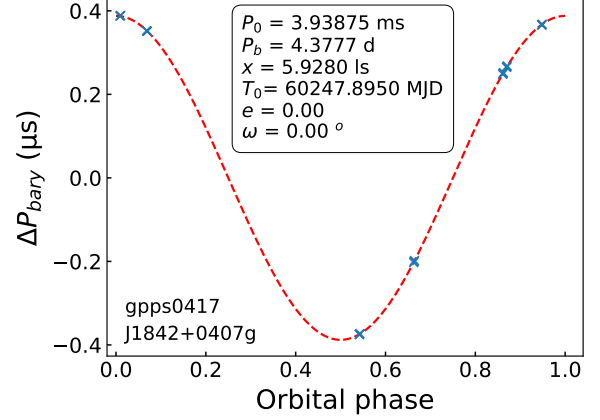


Figure 1. Variation of the barycentric periods for PSR J1842+0407g across the orbit phase. For each pulsar, the observed barycentric periods are marked by “x” after the spin period P_0 is subtracted. The error-bars are marked but too small to see for most data. Dashed line is the best-fit by using the preliminary Keplerian model with orbital parameters (P_b , x , T_0 , e and ω) listed inside the panel. The orbital phase is referred to the periastron of the orbit. Plots for 76 newly discovered pulsars by the FAST GPPS survey are given in Fig. AA3 in the Appendix.

The 19-beam L-band receiver works at a central frequency of 1250 MHz with a bandwidth of ~ 500 MHz (Jiang et al. 2020). Radio signals from two orthogonal linear polarizations, X and Y, are sampled, channelized and correlated (XX, YY, $\text{Re}[X^*Y]$, $\text{Im}[X^*Y]$) in digital backends for each beam. The data stream are stored in “SEARCH MODE” PSRFITS files with 2048 spectral channels and a time resolution of 49.152 μs in our observations.

The GPPS survey observations take 5 minutes for each pointing (Han et al. 2021). The verification observations of a pulsar take 15 minutes for the targeted objects by using the central beam (M01) of the 19-beam L-band receiver if it has been detected in any survey beam. In tracking observations the data from all 19 beams are also recorded. Sometimes we do detect some other pulsars from away beams (Han et al. 2024). In general, at the beginning or the end of each observation session, the periodic calibration noise signals are often turned on and off for 40 second or 1 minute or 2 minutes, which are used for the flux and polarization calibrations during off-line data processing.

Table 3. Binary parameters of 112 GPPS pulsars.

Pulsar (1)	RA (h:m:s) (2)	DEC (d:m:s) (3)	DM (cm^{-3} pc) (4)	P (ms) (5)	P_b (d) (6)	x (lt-s) (7)	e (8)	f (M_\odot) (9)	$m_{c,\text{min}}$ (M_\odot) (10)	$m_{c,\text{med}}$ (M_\odot) (11)	Comp. (12)	Ref. & Notes (13)
J0416+5201 (gpps0560)	04:16:27.277	+52:01:25.76	140.49	18.2405567	0.3964694	3.50556	4.6×10^{-5}	0.2943	1.261	1.568	CO/ONe	[1]
J0520+3722 (gpps0538)	05:20:13.564	+37:22:09.53	88.98	7.9132611	0.5796755	3.37242	1.0×10^{-6}	0.1226	0.837	1.019	CO/ONe	[1]
J0528+3529 (gpps0537)	05:28:28.798	+35:29:36.87	111.83	78.2336757	11.7261802	31.43462	0.290	0.2425	1.148	1.420	NS	[0]
J0622+0339 (gpps0388)	06:22:19.486	+03:39:42.88	79.41	8.7715338	9.5462660	4.89181	1.1×10^{-5}	1.379×10^{-3}	0.146	0.170	He	[0]
J1840+0012 (gpps0146)	18:40:49.206	+00:12:30.00	100.84	5.3389731	0.3285676	0.52890	3.5×10^{-5}	1.471×10^{-3}	0.149	0.174	He	[0]
J1844-0128 (gpps0555)	18:44:20.995	-01:28:25.77	368.18	29.1444223	10.6003185	20.96778	0.235	8.809×10^{-2}	0.724	0.876	NS	[0]
J1844+0028 (gpps0109)	18:44:37.359	+00:28:12.58	181.09	3.5706717	1.0788953	1.05955	4.9×10^{-5}	1.097×10^{-3}	0.134	0.156	He	[0]
J1845+0201 (gpps0547)	18:45:03.077	+02:01:49.36	56.65	4.3092504	5.3257088	4.55180	1.7×10^{-5}	3.570×10^{-3}	0.205	0.240	He	[0]
J1857+0642 (gpps0236)	18:57:58.678	+06:42:30.65	21.58	3.5309897	6.7345218	8.78290	6.6×10^{-6}	1.604×10^{-2}	0.361	0.427	CO/He	[0]
J1901+0658 (gpps0001)	19:01:22.851	+06:58:24.13	125.88	75.7438504	14.4547720	32.40203	0.366	0.1748	0.984	1.207	NS	[2]
J1903+0839 (gpps0100)	19:03:51.845	+08:39:17.19	166.45	4.6211691	0.3126397	0.40500	5.6×10^{-6}	7.297×10^{-4}	0.116	0.135	He	[0]
J1904+0553 (gpps0039)	19:04:16.822	+05:53:53.61	164.27	4.9073237	1.5836259	1.41774	6.7×10^{-6}	1.220×10^{-3}	0.139	0.163	He	[0]
J1905+0649 (gpps0229)	19:05:05.257	+06:49:49.33	187.66	27.4644124	1.3817147	6.62159	2.5×10^{-5}	0.1633	0.953	1.168	CO/ONe	[0]
J1908+1036 (gpps0114)	19:08:21.521	+10:36:35.36	10.91	10.6901954	3.9641259	11.38825	6.9×10^{-7}	0.1009	0.768	0.932	CO/ONe	[0]
J1911+1253 (gpps0181)	19:11:28.699	+12:53:17.41	68.68	27.2387038	11.7890531	20.43727	0.005	6.595×10^{-2}	0.639	0.770	CO/ONe	[0]
J1912+1416 (gpps0169)	19:12:30.513	+14:16:23.67	66.66	3.1662413	0.2468944	0.32981	1.1×10^{-5}	6.319×10^{-4}	0.110	0.129	He	[0]
J1916+0740 (gpps0166)	19:16:15.432	+07:40:41.17	219.86	11.2196601	14.8184145	7.31559	2.1×10^{-5}	1.914×10^{-3}	0.164	0.191	He	[0]
J1917+0615 (gpps0460)	19:17:20.288	+06:15:29.19	172.47	3.9676994	4.6184374	3.55159	4.6×10^{-5}	2.255×10^{-3}	0.174	0.203	He	[0]
J1917+1259 (gpps0012)	19:17:21.337	+12:59:59.82	117.01	5.6374684	3.2012644	5.89628	4.8×10^{-5}	2.148×10^{-2}	0.404	0.480	CO/He	[0]
J1918+0621 (gpps0494)	19:18:00.606	+06:21:59.38	63.11	2.1036826	4.4491966	2.73700	4.2×10^{-5}	1.112×10^{-3}	0.135	0.157	He	[0]
J1919+1341 (gpps0215)	19:19:23.012	+13:41:09.28	394.56	11.6557224	0.3703382	2.34094	1.0×10^{-5}	0.1004	0.766	0.930	CO/ONe	[1]
J1924+1342 (gpps0032)	19:24:16.597	+13:42:50.07	98.34	5.7210859	3.5281740	1.60733	4.8×10^{-6}	3.582×10^{-4}	0.091	0.105	He	[0]
J1928+1815 (gpps0121)	19:28:08.349	+18:15:30.26	346.14	10.5494991	0.1499024	1.69862	8.6×10^{-6}	0.2342	1.129	1.395	He MS	[3], Eclipse
J1930+1403 (gpps0013)	19:30:17.620	+14:03:53.80	150.48	3.2094483	5.5749284	5.18040	1.9×10^{-5}	4.803×10^{-3}	0.229	0.269	He	[0]
J1932+2121 (gpps0403)	19:32:21.201	+21:21:06.78	192.10	14.2447035	0.0809057	0.16269	2.8×10^{-5}	7.063×10^{-4}	0.115	0.134	MS	[0], Eclipse
J1936+2035 (gpps0197)	19:36:38.307	+20:35:47.29	198.86	32.9276838	1.0641434	5.64685	5.3×10^{-5}	0.1707	0.973	1.193	CO/ONe	[0]
J1938+2302 (gpps0392)	19:38:11.630	+23:02:00.16	303.36	52.7617558	33.9698770	54.67080	4.0×10^{-4}	0.1520	0.922	1.129	CO/ONe	[0]
J1943+2206 (gpps0514)	19:43:43.648	+22:06:33.26	211.10	4.6816713	26.7624656	23.79641	3.3×10^{-5}	2.020×10^{-2}	0.395	0.468	CO/He	[0]
J1943+2210 (gpps0227)	19:43:53.777	+22:10:33.97	110.66	12.8700790	0.3720527	2.57981	1.7×10^{-6}	0.1332	0.869	1.060	CO/ONe	[1]
J1946+0904 (gpps0242)	19:46:56.870	+09:04:53.33	37.18	25.7722599	6.0379626	7.13524	3.4×10^{-4}	1.070×10^{-2}	0.309	0.364	CO/ONe	[0]
J1947+2011 (gpps0011)	19:47:47.713	+20:11:00.45	127.49	8.1775519	81.9689107	37.80393	1.4×10^{-4}	8.634×10^{-3}	0.285	0.335	He	[0]
J1947+2304 (gpps0379)	19:47:28.937	+23:04:15.30	320.99	10.8936918	0.3388818	2.39708	1.6×10^{-5}	0.1288	0.856	1.043	CO/ONe	[1]

Table 3 continued

Table 3 (continued)

Pulsar	RA (h:m:s) (2)	DEC (d:m:s) (3)	DM (cm ⁻³ pc) (4)	P (ms) (5)	P _b (d) (6)	x (lt-s) (7)	e (8)	f (M _⊙) (9)	m _{c,min} (M _⊙) (10)	m _{c,med} (M _⊙) (11)	Comp. (12)	Ref.& Notes (13)
J1952+2837 (gpps0064)	19:52:49.653	+28:37:12.91	313.17	18.0209426	0.8674946	1.66242	8.1×10 ⁻⁶	6.555×10 ⁻³	0.257	0.302	CO/He	[0]
J1953+1844 (gpps0190)	19:53:37.946	+18:44:54.31	113.11	4.4440809	0.0370398	0.00666	5.5×10 ⁻⁴	2.312×10 ⁻⁷	0.0075	0.0087	UL	[4]
J2018+3518 (gpps0393)	20:18:48.149	+35:18:45.85	266.99	31.3162193	3.3327156	12.44297	4.3×10 ⁻⁵	0.1862	1.013	1.245	CO/ONe	[0]
J2023+2853 (gpps0201)	20:23:21.063	+28:53:41.45	22.75	11.3289050	0.7182304	4.00222	1.3×10 ⁻⁵	0.1334	0.869	1.061	CO/ONe	[1]
J0408+4955g (gpps0638)	04:08:07	+49:55	73.7	11.44457	2.9910	9.9122	-	0.1169	0.819	0.997	CO/ONe	
J0541+2959g (gpps0535)	05:41:44	+29:59	67.3	3.20648	0.3754	0.2289	-	9.138×10 ⁻⁵	0.057	0.066	UL	
J1814+0045g (gpps0549)	18:14:10	+00:45	124.0	2.30854	0.2023	0.1477	-	8.453×10 ⁻⁵	0.055	0.064	UL	Eclipse
J1819+0050g (gpps0581)	18:19:30	-00:50	103.3	6.60125	8.8132	17.6135	-	7.554×10 ⁻²	0.677	0.817	CO/ONe	
J1821+0007g (gpps0613)	18:21:02	+00:07	55.2	4.22205	8.0000	5.5350	-	2.845×10 ⁻³	0.189	0.221	He	
J1821+0044g (gpps0591)	18:21:31	+00:44	126.8	2.71314	2.3158	1.7697	-	1.110×10 ⁻³	0.135	0.157	He	
J1829+0235g (gpps0599)	18:29:35	-02:35	103.3	7.42749	0.9680	1.0035	-	1.158×10 ⁻³	0.137	0.160	He	
J1830+0106g (gpps0409)	18:30:07	-01:06	149.4	1.75841	0.1066	0.0810	-	5.021×10 ⁻⁵	0.046	0.053	UL	
J1833+0046g (gpps0365)	18:33:53	-00:46	81.4	2.95373	55.3724	13.7231	-	9.050×10 ⁻⁴	0.125	0.146	He	
J1835+0011g (gpps0221)	18:35:46	-00:11	36.2	3.22936	7.1903	5.8878	-	4.239×10 ⁻³	0.218	0.256	He	
J1835+0158g (gpps0636)	18:35:22	+01:58	181.5	3.31989	12.7241	9.1303	-	5.048×10 ⁻³	0.233	0.274	He	
J1836+0150g (gpps0394)	18:36:05	-01:50	199.5	5.45772	51.4903	21.5515	-	4.054×10 ⁻³	0.215	0.252	He	
J1837+0528g (gpps0204)	18:37:40	+05:28	120.8	6.25958	21.7247	16.4399	-	1.011×10 ⁻²	0.302	0.356	He	
J1838+0022g (gpps0107)	18:38:23	+00:22	122.6	5.08713	8.4150	2.6471	-	2.812×10 ⁻⁴	0.083	0.097	He	
J1838+0028g (gpps0350)	18:38:31	+00:28	107.3	1.86540	7.5914	8.9852	-	1.352×10 ⁻²	0.338	0.399	CO/He	
J1838+1507g (gpps0245)	18:38:36	+15:07	54.7	3.81818	0.1119	0.0512	-	1.151×10 ⁻⁵	0.028	0.032	UL	
J1839+0100g (gpps0419)	18:39:27	+01:00	130.1	5.36859	87.6694	32.1057	-	4.623×10 ⁻³	0.226	0.265	He	
J1842+0138g (gpps0565)	18:42:31	-01:38	209.9	2.70823	1.0943	1.0044	-	9.061×10 ⁻⁴	0.125	0.146	He	
J1842+0407g (gpps0417)	18:42:11	+04:07	101.6	3.93875	4.3777	5.9280	-	1.167×10 ⁻²	0.319	0.377	He/CO/ONe	
J1845+0104g (gpps0224)	18:45:50	+01:04	95.0	6.71355	3.9401	3.3096	-	2.507×10 ⁻³	0.180	0.211	He	
J1845+0315g (gpps0566)	18:45:18	+03:17	77.3	1.85070	0.1901	0.0150	-	1.003×10 ⁻⁷	0.006	0.007	UL	
J1846+0507g (gpps0614)	18:46:50	+05:07	101.6	3.07255	19.4795	11.2908	-	4.073×10 ⁻³	0.215	0.252	He	
J1847+0342g (gpps0431)	18:47:30	+03:42	81.1	4.28904	0.1392	0.0360	-	2.585×10 ⁻⁶	0.017	0.020	UL	
J1849+0304g (gpps0342)	18:49:32	+03:04	146.7	1.79342	0.2412	0.7614	-	8.146×10 ⁻³	0.278	0.328	MS	
J1849+0623g (gpps0485)	18:49:50	+06:23	129.2	14.58764	6.9840	11.6331	-	3.465×10 ⁻²	0.489	0.584	CO/ONe	
J1852+0309g (gpps0171)	18:52:10	+03:09	358.0	5.57677	1.5774	1.2909	-	9.283×10 ⁻⁴	0.126	0.147	He	
J1853+0008Ag (gpps0193)	18:53:12	-00:08	285.2	2.82485	77.9991	28.3801	-	4.034×10 ⁻³	0.215	0.252	He	
J1854+0012g (gpps0020)	18:54:16	+00:13	204.1	2.70923	7.4103	5.5362	-	3.318×10 ⁻³	0.200	0.234	He	
J1856+1000g (gpps0331)	18:56:30	+10:00	202.1	4.86584	10.5916	2.2154	-	1.041×10 ⁻⁴	0.059	0.069	UL	
J1857+0125g (gpps0396)	18:57:21	-01:25	213.9	1.83371	0.2385	0.5575	-	3.271×10 ⁻³	0.199	0.233	He/MS	
J1857+0230g (gpps0577)	18:57:20	-02:30	134.5	35.15683	29.4902	53.7076	-	0.1913	1.026	1.262	CO/ONe	

Table 3 continued

Table 3 (continued)

Pulsar	RA (h:m:s)	DEC (d:m:s)	DM (cm^{-3} pc)	P (ms)	P_b (d)	x (lt-s)	e	f (M_\odot)	$m_{c,\text{min}}$ (M_\odot)	$m_{c,\text{med}}$ (M_\odot)	Comp.	Ref.& Notes
(1)	(2)	(3)	(4)	(5)	(6)	(7)	(8)	(9)	(10)	(11)	(12)	(13)
J1858-0128g (gpps0425)	18:58:11	-01:28	38.1	7.87566	96.9722	42.0315	-	8.487×10^{-3}	0.283	0.333	He	
J1858+0244g (gpps0125)	18:58:01	+02:44	282.7	2.61247	91.6645	25.8920	-	2.218×10^{-3}	0.173	0.202	He	
J1859+0026Ag (gpps0066)	18:59:58	+00:26	334.1	8.57234	95.1021	40.3135	-	7.778×10^{-3}	0.274	0.322	He	
J1859+0313g (gpps0131)	18:59:35	+03:13	107.8	1.61335	0.4443	1.1770	-	8.869×10^{-3}	0.288	0.339	MS	Eclipse
J1859+0658g (gpps0162)	18:59:04	+06:58	290.4	5.11175	9.2967	6.9825	-	4.229×10^{-3}	0.218	0.256	He	
J1900+0213g (gpps0063)	19:00:12	+02:13	309.9	32.09151	826.6043	309.3251	-	4.651×10^{-2}	0.552	0.662	CO/He	
J1903+0830g (gpps0531)	19:03:39	+08:30	334.8	4.08534	6.0782	4.4347	-	2.535×10^{-3}	0.181	0.212	He	
J1904+0836g (gpps0104)	19:04:35	+08:36	90.5	4.43642	6.0242	4.9921	-	3.681×10^{-3}	0.207	0.243	He	
J1907+0009g (gpps0588)	19:07:21	+00:09	83.0	2.37558	6.1895	5.0710	-	3.655×10^{-3}	0.207	0.243	He	
J1907+0014g (gpps0579)	19:07:56	+00:14	172.6	24.51782	4.0846	15.5954	-	0.2441	1.152	1.425	CO/ONe	
J1907+0052g (gpps0600)	19:07:57	+00:52	162.9	2.92067	6.1830	3.1321	-	8.630×10^{-4}	0.123	0.114	He	
J1908+0029g (gpps0633)	19:08:30	+00:29	165.3	3.41581	2.0753	2.0276	-	2.078×10^{-3}	0.169	0.197	He	
J1908+0705g (gpps0278)	19:08:55	+07:04	41.4	1.99057	0.8509	0.9260	-	1.177×10^{-3}	0.138	0.161	He	
J1908+0949g (gpps0128)	19:08:07	+09:49	220.1	9.04837	2.8725	3.8534	-	7.446×10^{-3}	0.269	0.317	He/CO	
J1910+0423g (gpps0432)	19:10:10	+04:23	339.9	93.24143	893.6631	222.6467	-	1.484×10^{-2}	0.350	0.414	He/CO	
J1910+1054g (gpps0049)	19:10:01	+10:54	139.3	3.87080	65.4001	28.4605	-	5.787×10^{-3}	0.245	0.288	He	
J1911+1206g (gpps0235)	19:11:24	+12:06	181.7	3.44012	0.1724	0.0150	-	1.294×10^{-7}	0.006	0.007	UL	
J1915+0720g (gpps0413)	19:15:35	+07:20	122.1	5.69055	4.5372	3.3045	-	1.882×10^{-3}	0.163	0.190	He	
J1917+1046g (gpps0157)	19:17:55	+10:46	163.1	87.73271	827.99	236.13	-	2.062×10^{-2}	0.398	0.472	He/CO	
J1918+1536g (gpps0145)	19:18:23	+15:36	123.4	109.93966	20.5750	31.5020	-	7.929×10^{-2}	0.691	0.835	CO/ONe	
J1918+1540g (gpps0144)	19:18:19	+15:40	271.1	4.28381	14.8603	19.7143	-	3.725×10^{-2}	0.504	0.602	CO/ONe	
J1918+1547g (gpps0160)	19:18:34	+15:47	64.6	3.76417	4.6734	4.0298	-	3.217×10^{-3}	0.197	0.231	He	
J1919+0126g (gpps0383)	19:19:23	+01:26	125.2	1.89736	0.2694	0.0806	-	7.746×10^{-6}	0.024	0.028	UL	
J1919+1502g (gpps0411)	19:19:57	+15:02	232.8	3.64606	0.1119	0.1686	-	4.110×10^{-4}	0.095	0.110	MS	
J1921+1216g (gpps0237)	19:21:03	+12:16	256.2	3.00144	8.4166	6.0642	-	3.380×10^{-3}	0.201	0.236	He	Eclipse
J1921+1652g (gpps0336)	19:21:34	+16:52	124.1	3.68199	2.7022	1.6514	-	6.622×10^{-4}	0.112	0.131	He	
J1923+2022g (gpps0155)	19:23:46	+20:22	175.3	37.99289	776.4691	243.6075	-	2.575×10^{-2}	0.434	0.517	CO/He	
J1928+1458g (gpps0262)	19:28:42	+14:58	86.2	2.97268	18.3944	13.9841	-	8.678×10^{-3}	0.285	0.336	He	
J1928+1902g (gpps0163)	19:28:05	+19:02	28.9	5.79515	18.7472	20.0607	-	2.466×10^{-2}	0.427	0.508	CO	
J1929+1259g (gpps0345)	19:29:50	+12:59	90.9	2.85359	50.0942	23.8465	-	5.802×10^{-3}	0.245	0.288	He	
J1929+2355g (gpps0239)	19:29:44	+23:55	206.8	4.79296	10.1584	8.3292	-	6.012×10^{-3}	0.249	0.292	He	
J1930+1708g (gpps0274)	19:30:17	+17:08	87.2	2.27626	12.0134	7.3907	-	3.003×10^{-3}	0.193	0.226	He	
J1931+1428g (gpps0474)	19:31:48	+14:28	241.3	2.60770	0.1815	0.5682	-	5.979×10^{-3}	0.248	0.292	MS	Eclipse
J1936+1952g (gpps0065)	19:36:00	+19:52	325.3	9.72399	15.5908	8.5568	-	2.780×10^{-3}	0.187	0.219	He	
J1939+1848g (gpps0500)	19:39:01	+18:48	79.3	3.35659	11.9875	10.5015	-	8.653×10^{-3}	0.285	0.336	He	

Table 3 continued

Table 3 (continued)

Pulsar	RA (h:m:s) (2)	DEC (d:m:s) (3)	DM (cm^{-3} pc) (4)	P (ms) (5)	P_b (d) (6)	x (lt-s) (7)	e (8)	f (M_\odot) (9)	$m_{c,\text{min}}$ (M_\odot) (10)	$m_{c,\text{med}}$ (M_\odot) (11)	Comp. (12)	Ref.& Notes (13)
J1940+2102g (gpps0564)	19:40:13	+21:02	76.3	30.04720	15.2938	31.2624	-	0.1403	0.889	1.086	CO/ONe	
J1943+2446g (gpps0434)	19:43:20	+24:46	237.3	5.59015	32.9876	11.2280	-	1.413×10^{-3}	0.147	0.171	He	
J1943+2847g (gpps0416)	19:43:36	+28:47	191.6	6.29597	12.9530	9.1491	-	4.901×10^{-3}	0.230	0.271	He	
J1952+2702g (gpps0054)	19:52:18	+27:02	213.1	4.14230	10.7125	8.1495	-	5.064×10^{-3}	0.233	0.274	He	
J1953+1006g (gpps0243)	19:53:34	+10:06	57.2	2.58559	0.1204	0.0225	-	8.437×10^{-7}	0.012	0.013	UL	Eclipse
J1957+2711g (gpps0562)	19:57:36	+27:11	210.4	23.37711	11.5406	24.7921	-	0.1228	0.838	1.020	CO	
J2000+3157g (gpps0590)	20:00:03	+31:57	270.0	3.49855	29.2071	18.2898	-	7.701×10^{-5}	0.273	0.321	He	
J2003+3032g (gpps0271)	20:03:53	+30:32	164.4	1.78537	0.1495	0.0677	-	1.491×10^{-5}	0.031	0.035	UL	
J2007+3343g (gpps0604)	20:07:53	+33:43	217.2	2.68151	1.8900	1.2175	-	5.425×10^{-4}	0.105	0.122	He	
J2015+3404g (gpps0544)	20:15:14	+34:04	208.0	4.27779	50.6152	26.4768	-	7.779×10^{-3}	0.274	0.322	He	

NOTE—Pulsar name with the GPPS number in the bracket; right ascension (RA, in hh:mm:ss.s); declination (Dec, in dd:mm:ss.s), dispersion

measure (DM, in pc cm^{-3}); pulsar spin period P (in second); orbital period P_b (in days); projected semi-axis x (in light year); orbital eccentricity e ; mass function f ; the minimum and median companion mass $m_{c,\text{min}}$ and $m_{c,\text{med}}$ of the companion estimated by assuming the orbit inclination angle of $i = 90^\circ$ or 60° together with the pulsar mass $m_p = 1.35M_\odot$; Companion types: He-white dwarf (He WD), CO/ONe white dwarf (CO/ONe WD), neutron star (NS), main sequence star (MS), ultra light object or palent (UL); Notes: Eclipse for eclipsing pulsar.

References—[0]: this work; [1]: Yang et al. (2024a); [2]: Su et al. (2024); [3]: Yang et al. (2024b); [4]: Pan et al. (2023).

Table 4. Measured and derived parameters of PSR J0528+3529, as one example of 27 pulsars with phase-connected timing solutions presented in Table A A1.

Pulsar name	J0528+3529
GPPS name	gpps0537
MJD range	59930-60625
Dat Span (yr)	1.9
Number of TOAs	23
Ref. epoch (MJD)	60000
Measured quantities	
Right ascension: RA (hh:mm:ss)	05:28:28.7978(1)
Declination: DEC (dd:mm:ss)	+35:29:36.81(3)
Dispersion measure: DM (cm ⁻³ pc) ..	111.837
Pulse frequency: ν (s ⁻¹)	12.78221930378(2)
First derivative $\dot{\nu}$: $\dot{\nu}$ (10 ⁻¹⁶ Hz s ⁻¹) ..	-1.202(4)
Residual (μ s)	6.037
EFAC	0.77
EQUAD	0.0
Reduced χ^2	0.99
Binary parameters	
Binary model	DD
Orbital period: P_b (d)	11.7261813(4)
Projected semi-major axis: x (lt-s) ..	31.43468(2)
Periastron passage time: T_0 (MJD) ..	59994.190822(8)
Orbital eccentricity: e	0.2901088(10)
Longitude of periastron: ω (deg)	184.9436(2)
Advance rate of ω : $\dot{\omega}$ (deg/yr)	0.0072(3)
Derived quantities	
Galactic longitude: l (deg)	172.52387(3)
Galactic latitude: b (deg)	0.46700(2)
YMW17 ¹ distance: D_{YMW} (kpc) ...	1.933
NE2001 ² distance: D_{NE2001} (kpc) ..	2.950
Spin period: P (ms)	78.23367572047(12)
Derivative of P : \dot{P} (10 ⁻²¹ s s ⁻¹) ...	736(2)
Characteristic age: τ (Gyr)	1.686
Surface magnetic field: B_{surf} (10 ⁸ G)	76.762

NOTE— Ephemeris obtained based on the DE440 solar system model (Park et al. 2021), Barycentric Dynamical Time (TDB) units, and TT(TAI) clock. Distances estimated by YMW16 model Yao et al. (2017) or NE2001 Cordes & Lazio (2002).

2.1. Data reduction

With the initial period and DM obtained from the GPPS survey, we fold the survey data and initial follow-up FAST observation data by using DSPSR³ (van Straten & Bailes 2011). The optimal barycentric period P_{bary} for each observation is first searched from a set of trial periods around its nominal value by using the PDMP tool from PSRCHIVE⁴ (Hotan et al. 2004). For a binary pulsar, the observed P_{bary} varies due to the Doppler effect caused by orbital motion (e.g. Freire et al. 2001). Its initial orbital parameters are obtained by grid searching over the two dimensional parameter space of the orbital period P_b and the epoch of passage of periastron T_0 , together with fitting for the projected semi-major

axis x and spin period P_0 . By combing orbital period P_b and projected semi-axis x , one can get the mass function f ,

$$f(m_p, m_c) = \frac{(m_c \sin i)^3}{(m_p + m_c)^2} = \frac{4\pi^2 x^3}{T_\odot P_b^2}. \quad (1)$$

Here, m_p and m_c are the masses for pulsar and the companion, i is the inclination angle of binary orbit, $T_\odot = GM_\odot/c^3 = 4.925490947\mu\text{s}$ with G the gravitational constant and c the speed of light. Then the median companion masses can be obtained assuming $m_p = 1.35 M_\odot$ and $\sin i = 60^\circ$. These parameters are further refined with FITORBIT⁵, during which the orbital eccentricity e and longitude of periastron ω might also be obtained. With this approach, preliminary orbital parameters are obtained for all the binaries systems, as shown in Figure 1 as an example.

Some binary pulsars are monitored for years after initial discoveries by the GPPS survey. Further timing analysis is performed in the following steps. The ELL1 or DD model is first employed to model the orbital motion, depending on if xe^2 is much less or larger than the uncertainty of the time of arrival, because one can not reliably define the time and location of periastron for a nearly circular orbit. The covariance can be avoided by the Laplace-Lagrange eccentricity parameterizations by using $\epsilon_1 = e \sin \omega$ and $\epsilon_2 = e \cos \omega$ (Lange et al. 2001). The ELL1 model is parameterized by P_b , x , T_{asc} , ϵ_1 and ϵ_2 . Here, $T_{\text{asc}} = T_0 - \omega P_b / 2\pi$ represents the epoch of the ascending node. The DD model is parameterized by P_b , x , T_0 , e and ω . These five Keplerian parameters of ELL1 or DD together with previously estimated pulsar position (α and δ), rotation period P and dispersion measure (DM) form the initial pulsar ephemeris.

With the initial ephemeris, we fold the data to form ‘‘FOLD MODE’’ PSRFITS archive files with DSPSR. After removing radio-frequency interference (RFI) using PAZ and PSRZAP, one can integrate all subintegrations and all channels using PAM in the PSRCHIVE tool and get a noise-free standard profile template by using PAAS. Then, we obtain TOAs from cross-correlating the template with all observed pulse profiles by using PAT. With the initial ephemeris and TOAs, phase coherent timing solution is obtained by determining the global rotational count through mapping the gaps between adjunct observations with DRACULA (Freire & Ridolfi 2018).

Using the phase-connected ephemeris, the recorded data are de-dispersed and folded again. They are calibrated in polarization following the procedures described by Wang et al. (2023). The whole frequency channels are summed one for data of every 5 minutes. New TOAs are extracted again. To account for the influence of white noise, ToA uncertainties are scaled by EFAC and quadratically added with EQUAD with the help of the efacEquad plugin of tempo2 (Hobbs et al. 2006). The ephemeris is finally refined to get a better param-

³ <http://dspsr.sourceforge.net/>

⁴ <http://psrchive.sourceforge.net>

⁵ <https://github.com/vivekvenkris/fitorbit>

Table 5. Pulsar polarization profile parameters of 27 new binary pulsars from added FAST observations based on pulsar ephemeris. Numbers in brackets are uncertainties on the last digit.

PSR	P	W_{50}	W_{10}	L/I	V/I	$ V /I$	RM
(1)	(ms)	($^{\circ}$)	($^{\circ}$)	(%)	(%)	(%)	(rad/m 2)
(1)	(2)	(3)	(4)	(5)	(6)	(7)	(8)
J0528+3529	78.233	6.6(7)	12.9(7)	10.2(31)	-5.0(31)	6.3(31)	-88(5)
J0622+0339	8.771	9.4(14)	-	49.7(38)	-13.4(36)	14.9(36)	28.9(15)
J1840+0012	5.338	193.7(14)	239.9(15)	36.2(31)	0.9(30)	6.9(31)	23.4(6)
J1844-0127	29.142	18(6)	-	-	-3(7)	4(7)	-
J1844+0028	3.571	61(3)	-	7.4(32)	9.2(32)	10.3(32)	-32(8)
J1845+0201	4.309	139(3)	156(3)	15.4(33)	-1.4(32)	5.1(32)	20(6)
J1857+0642	3.530	42.0(7)	173.4(7)	34.1(30)	-8.6(30)	12.9(30)	-30.7(11)
J1903+0839	4.621	41.5(7)	216.2(7)	21.1(30)	5.9(30)	10.0(30)	247.1(13)
J1904+0553	4.907	40.9(7)	138.4(7)	12.8(30)	10.6(30)	12.3(30)	-67.0(16)
J1905+0649	27.464	20(3)	-	-	5.5(49)	8.3(49)	-
J1908+1036	10.690	5.5(7)	26.1(7)	71.3(31)	-1.0(30)	1.3(30)	-27.2(8)
J1911+1253	27.238	25.6(7)	38.8(7)	5.3(31)	4.2(31)	11.8(31)	224(7)
J1912+1416	3.166	50.8(14)	82.6(14)	15.1(31)	-7.2(31)	10.9(31)	214.7(24)
J1916+0740	11.219	91.8(14)	255.9(15)	15.9(31)	-10.6(31)	12.9(31)	609(3)
J1917+0615	3.967	73.5(14)	-	18.6(32)	-11.5(31)	14.9(31)	11.4(18)
J1917+1259	5.637	20.6(14)	-	9.8(33)	4.0(33)	10.9(33)	247(14)
J1918+0621	2.103	14.3(14)	34.5(14)	25.2(30)	26.6(30)	27.3(30)	-88.7(8)
J1924+1342	5.721	69.8(28)	-	14.9(33)	-12.6(31)	16.7(31)	103(13)
J1930+1403	3.209	25.1(14)	51.9(14)	42.5(31)	2.2(31)	2.4(31)	59.4(7)
J1932+2121	14.244	12.1(7)	36.6(7)	16.1(30)	-8.4(30)	9.5(30)	99.5(10)
J1936+2035	32.927	17.1(14)	-	64.4(38)	-0.7(37)	7.0(37)	12.7(12)
J1938+2302	52.761	11.2(7)	-	7.1(33)	-2.2(33)	4.0(33)	66(8)
J1943+2206	4.681	20(3)	-	20(4)	5(4)	11(4)	-165(25)
J1946+0904	25.772	30.7(7)	64.4(7)	19.8(30)	4.1(30)	5.0(30)	-105.3(6)
J1947+2011	8.177	9.1(7)	27.5(7)	7.8(32)	11.7(32)	13.6(32)	-48(8)
J1952+2837	18.020	21.1(7)	159.8(7)	21.4(30)	9.7(30)	11.2(30)	-42.5(5)
J2018+3518	31.316	20.3(28)	-	42.2(40)	5.7(35)	3.9(35)	-332(7)

NOTE— Columns (1)-(2): pulsar name; spin period, Columns (3)-(8): the profile properties: pulse widths W_{50} and W_{10} at 50% and 10% the peak intensities, degree (and uncertainty on the last digit) of linear, circular and absolute circular polarization L/I , V/I and $|V|/I$; FAST measured RM (and uncertainty), i.e. $RM_{ISM} = RM_{obs} - RM_{ion}$. Column (9)-(11): α_0 : inclination angle of the magnetic axis with respect to the rotation axis, β_0 : impact angle for the closest approach of a sight line with respect to the magnetic axis, Features: S: S-shaped position angle; ot: orthogonal modes; hiL: highly linearly polarized; hiC: highly circularly polarized; ip: interpulse; w: wide profile; c: scattering.

eter estimation with $\chi^2 \sim 1$. One example is given in Table 4, and the ephemeris of 27 pulsars in Table AA1.

2.2. Pulsar polarization profiles

Pulsar polarized pulse profile represents the mean radiation feature of each pulsar. It is obtained by integrating the emission of tens of thousands of individual pulses. Data from multiple timing observations are then combined to form the integrated pulse profiles, as shown in Figure 2 for PSR J1952+2836 as an example. Polarization profiles for 27 pulsars are shown in Figure AA2. The profile width at 50% and 10% the peak intensity, the fractional linear, circular and absolute circular polarization are measured and listed in columns (3) to (7) of Table 5. The rotation measures (RM) are listed in column (8). Emission features of these profiles are indicated in the last column.

These pulsars are generally MSPs with wide profiles. The widths of their profiles range from 12.9 $^{\circ}$ to 255.9 $^{\circ}$ at 10% the peak intensity. Profiles of PSRs J1840+0012 and

J1916+0741 are extreme wide, emissions of which extend to more than 180 $^{\circ}$. PSRs J1903+0839 and J1932+2121 exhibit inter pulse emissions that separate by about 180 $^{\circ}$ from the main pulses. PSRs J1840+0012, J1857+0642, J1916+0740, J1930+1403 and J1946+0904 have a S-shaped position angle variations. PSRs J0528+3529, J1857+0642, J1903+0839, J1904+0553, J1916+0741, J1946+0904 and J1952+2836, exhibit orthogonal modes manifesting as 90 $^{\circ}$ position angle jumps. The leading component of PSRs J1857+0642 and J1916+0741, the inter pulse of PSR J1903+0839 and the profile of J1908+1035 are highly linearly polarized. PSRs J1936+2035 and J2018+3518 are affected by interstellar scattering, which results in scattering tails of profiles together with flat PAs. These diverse polarization properties resemble those categories reported in Wang et al. (2023).

3. DETAILED RESULTS OF VARIOUS BINARY PULSARS

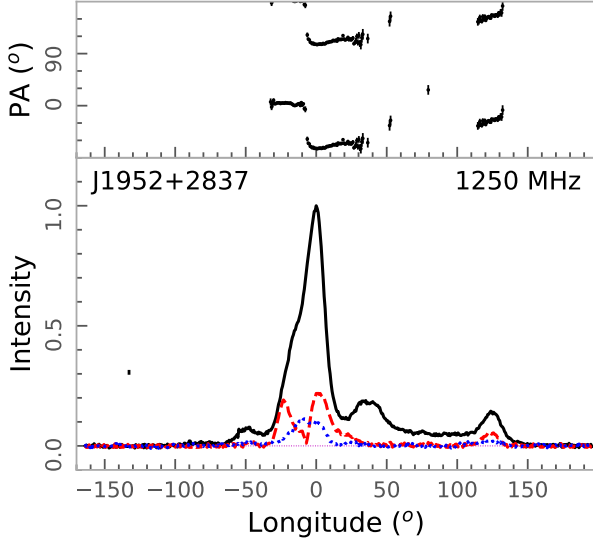


Figure 2. Integrated pulse profiles of PSR J1952+2837. The total intensity, linear and circular polarization are represented by solid, dashed and dotted lines in the bottom sub-panel. The left-hand circular polarization is defined to be positive. The bin size and 3σ are marked inside the sub-panel, here σ is the standard deviation of off-pulse bins. In the top panel, dots with error-bar are measurements of polarization position angles for linear polarization intensity exceeding 3σ line. The position angles are corrected to infinite frequency by discounting Faraday rotation. Polarized pulse profiles of the 27 pulsars are shown in Figure AA2.

Table 6. Population and companion statistics for pulsar binaries.

Binary pulsars	Known Binaries			FAST GPPS	
	GF	GC	EC	GF	GC
Total	420			112	
Location	GF	GC	EC	GF	GC
	315	104	1	111	1
He-WD	129	23	-	56	-
CO/ONe-WD	39	3	-	23	-
Ultra light object	42	26	-	11	1
Main sequence star	22	5	1	5	-
Neutron star	17	2	-	3	-
Giant star	1	-	-	-	-
Helium star	-	-	-	1	-
uncertain	65	45	-	12	-

NOTE—GF, GC and EG are for Galactic field, Globular clusters and extra galaxy, respectively. The known pulsar binaries are from ATNF pulsar Catalogue 2.4.0 (Manchester et al. 2005). It incorporates 3 triple systems with two having He-WD and one having UL companions.

More than 160 binary pulsars have been found by the FAST GPPS survey. We have got 9 pulsars published (Su et al. 2024; Pan et al. 2023; Yang et al. 2023, 2024a,b), as mentioned at the end of introduction. For 6 binary pulsars, PSRs J0653+0443, J1852–0044, J1856–0039, J1921+1631,

J1922+1511 and J1933+2038, we have obtained the time solutions and are preparing independent papers. Here we list 112 pulsars in Table 3. The table consists of two parts, the first for pulsars with phase-connected timing solution, and the second part for pulsars without solutions. There are 36 pulsars in the first part, including the 9 published pulsars for completeness. For these 36 pulsars, we listed in the first part of Table 3 their names, right ascension, declination and dispersion measure in columns (1), (2), (3) and (4). Spin period P obtained from discovery is refined from modeling the orbital motion, as listed in column (5). Columns (6), (7) and (8) are for orbital period P_b , projected semi-axis x , and orbital eccentricity e obtained by modeling the Keplerian orbit. Mass functions of these binary systems are listed in column (9) of Table 3. By assuming $i = 90^\circ$ or 60° and $m_p = 1.35M_\odot$, the minimum and median companion mass are estimated, as listed in columns (10) and (11). With the spin period, orbital period, eccentricity and the rough companion mass, the companion type can be roughly estimated, as listed in column (13) of Table 3. The new ephemeris with measured and derived parameters for 27 pulsars are given in details in Appendix Table AA1 and one example is shown in Table 4. The timing residuals are shown for two pulsars in Figure 3 and for all 27 pulsars in Figure AA1, which are plotted along the observation epochs and versus the orbital phase. Timing residuals range from 1.053 to 174.563 μs .

For the other 76 pulsars, we have not yet got the timing solution from the limited number of observations, but we get the currently best-fitted preliminary Keplerian parameters obtained from available FAST observations made by the FAST GPPS survey or follow-up tracking observations in applied projects. Their positions have not been well determined yet, so their temporal names have “g” at the end.

The companions of binary pulsars are diverse (see Table 6). The ranges of P , P_b , $m_{c,med}$ and e are listed in Table 1 for the binary pulsars with different types of companions in the Galactic field. Criteria for their classification is demonstrated in the last column. Companion type of a binary pulsar can be determined based mainly on the measured spin period (P), period derivative (\dot{P}), orbital period (P_b), orbital eccentricity (e) and the estimated companion mass ($m_{c,med}$) for a given binary system, as well as its distribution in the P_b v.s. $m_{c,med}$ and P_b v.s. e diagrams, as shown in Figure 5.

See Table 6 for the numbers of the GPPS binary pulsars with various companions. Their fractions are shown in Figure 4. It is apparent that the GPPS binaries have a significantly larger fraction of CO-WDs compared with the known population.

In the following we discuss the GPPS binary pulsars according to their probable companions.

3.1. Pulsars with He-WD companions

The pulsar He-WD binary systems are generally believed to be formed from the LMXBs via the Case A RLO which results in a fully recycled pulsar in an orbital period shorter than one day, or via the Case B RLO that results in a fully or partially recycled pulsar with an orbital period in the ranging

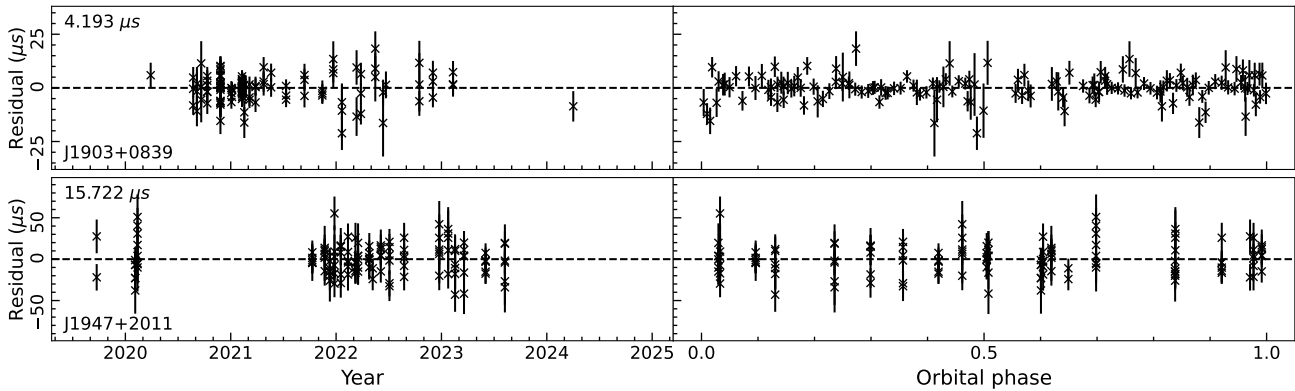


Figure 3. Timing residuals of two example pulsars PSR J1903+0839 and J1947+2011. *Left panels:* Residuals versus observation epochs. The weighted root-mean-square residual of each pulsar is indicated in the top left corner of the panel. *Right panels:* Residuals versus orbital phase. The orbital phases are referred to ascending node or periastron depending on the binary model of each pulsar. Timing residuals of the 27 binary pulsars are shown in Figure AA1.

from one to a thousand days (e.g. [Webbink et al. 1983](#); [Tauris & Savonije 1999](#); [Podsiadlowski et al. 2002](#); [Tauris & van den Heuvel 2023](#)). The pulsar He-WD binaries might also be evolved from the IMXBs when the Case A RLO is not initiated too late during the main-sequence evolution of the donor star (e.g. [Podsiadlowski et al. 2002](#)). Binary pulsars evolving in this channel are fully recycled and have orbital period between 3-20 days ([Tauris 2011](#)).

Pulsars with He-WD companions are generally fully recycled and hence have spin periods $P < 10$ ms with a lognormal distribution with the most probable spin period of about 3.5 ms, as shown in Figure 6. The orbital periods range from 0.1 day to several hundred days. As suggested by [Tauris et al. \(2012\)](#), the companion of a pulsar is most likely a He-WD if the median mass is in the range of $0.08M_{\odot} < m_{c,med} < 0.335M_{\odot}$ for a system with an orbital period of $P_b < 75$ days, or the median mass in the range of $0.08M_{\odot} < m_{c,med} < 0.46M_{\odot}$ for a system with an orbital period of $P_b > 75$ days.

We get 56 GPPS binary pulsars that most likely have He-WD companions. We have obtained timing solution for 13 such pulsars, but not yet for another 43 pulsars (see Table 3). Among the GPPS pulsars, 5 pulsars, PSRs J1840+0012, J1903+0839, J1912+1416, J1829-0235g and J1908+0705g, have orbital periods shorter than one day and exhibit no eclipsing as shown from observations. They are most likely formed via the Case A RLO from LMXBs. The other 51 MSPs have orbital periods longer than one day, and are most likely formed via the Case B RLO from LMXBs.

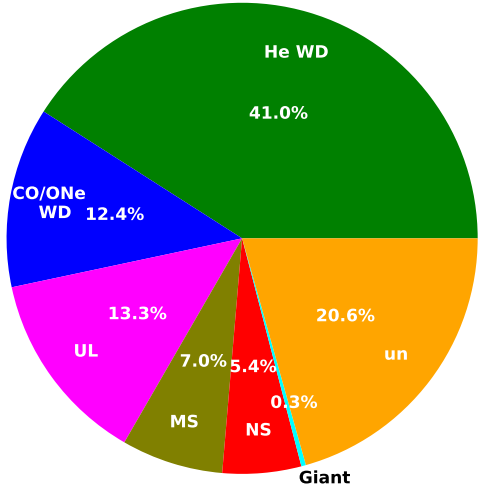
During the evolution, the recycling processes results in two fossil relations for the orbital parameters for MSPs if they have a low mass companion with an orbital period $P_b \geq 1$ day. One is P_b versus m_c ([Refsdal & Weigert 1971](#); [Tauris & Savonije 1999](#); [Istrate et al. 2014](#); [Antoniadis 2014](#)), as shown in Figure 5. The GPPS pulsars, e.g., PSRs J0622+0339, J1844+0028, J1904+0553, J1916+0740, J1917+0615, J1918+0621, J1930+1403 and J1947+2011, are around the relation, which is an indication for the companion type.

The other fossil relation is P_b versus e for He-WD binaries ([Phinney 1992](#)), as shown in Figure 5. Positive correlations between P_b and e are evident for pulsars with He companions with correlation coefficient of 0.66. This correlation is related to tides resulting from density fluctuations in the convective envelope, and systems with wider orbits during the mass transfer prevent perfect circularization ([Tauris & van den Heuvel 2023](#)). The GPPS pulsars, e.g., J1857+0642, J1943+2206 and J1947+2011, are consistent with the relation.

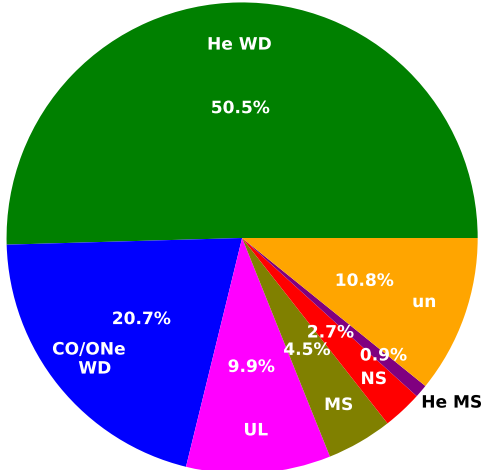
The distribution of orbital periods was noticed to have two gaps around $P_b \sim 25 - 50$ days (e.g. [Tauris 1996](#); [Taam et al. 2000](#)) and around $P_b \sim 2.5 - 4.5$ days ([Hui et al. 2018](#)). With the newly discovered GPPS binary pulsars, we see the peaks are enhanced, the gaps are confirmed with the lower boundary for the large gap extending from 25 to about 16 days, as shown in Figure 6.

3.2. Pulsars with CO/ONe-WD companions

A pulsar CO/ONe WD binary system can be formed from an IMXB via the Case A RLO in small orbits that results in a fully recycled pulsar with an orbital period of 3-20 days ([Podsiadlowski et al. 2002](#); [Tauris et al. 2011](#)), or via an early Case B RLO in a wider orbit that results in a partial recycled pulsar with an orbital period of 3-50 days ([Podsiadlowski et al. 2002](#)), or via the late Case B or Case C RLO and a common envelope in very wide orbits that result in a partial recycled pulsar with CO/ONe companion with an orbital period less than 20 days ([Ivanova et al. 2013](#); [Tauris & van den Heuvel 2023](#)). In addition, there are also systems that might be formed from LMXBs via the late Case B RLO ([Tauris & Savonije 1999](#)), which leads to a slowly spinning pulsar in an extremely wide orbit with orbital periods $\gtrsim 800$ days. The NS in such a system is only mildly recycled. Another possibility is that in a HMXB the star with a higher initial mass evolves into a massive WD instead of an NS due to mass ratio reversal ([Kaspi et al. 2000](#)). The NSs in these systems are non-recycled and their orbit are eccentric.



(a) 315 known binaries



(b) 111 GPPS binaries

Figure 4. Fractions of binary pulsars with different types of companions in the Galactic field. The top panel is for 315 known binaries and the bottom panel for the 111 GPPS discovered ones. Their numbers are listed in Table 6.

The companion of a pulsar is likely a CO/ONe WD when the pulsar has a spin period of $P > 8$ ms, the orbital eccentricity $e < 0.05$, an orbital period $P_b < 75$ days, together with the companion having the median mass $m_{c,med} > 0.335M_\odot$ (Tauris et al. 2012).

We have 23 binary pulsars discovered in the GPPS survey which probably have CO/ONe WD companions, as listed in Table 3. We have obtained timing solutions for 7 of them. Figure 7 shows the distribution of these pulsars in P vs P_b diagram. It is apparent that the binary pulsars with CO companions have a broad range of spin periods from as low as 2.9

ms to about 1.1 s, and have a most probable orbital period of about 10 days.

Among these systems, PSR J1908+1036 has the smallest eccentricity among all the pulsar CO-WD binary systems, though with large measurement uncertainty. The pulsar has a small DM of 10.91 pc cm^{-3} , which indicates that it is a nearby system. We do find the optical counterpart of the companion simply by inspecting manually of the images from the Pan-STARRS1 image cutout server⁶ with stack image at *grizyP1* bands, as shown in Figure 8. The detailed evolution history needs to be further investigated.

3.3. Pulsars with ultra-light companions

Some pulsars have an UL companion with a median mass $m_{c,med} < 0.08M_\odot$ (Manchester et al. 2005; Tauris et al. 2012). The UL companions are generally formed via the Case A RLO of LMXBs (Tauris & van den Heuvel 2023). Magnetic braking takes away their orbital momentum leading to compact orbits. Some of them, such as PSR J1953+1844 (Yang et al. 2023), undergo evolution from ultra-compact X-ray binaries (UCXBs), then to accreting X-ray millisecond pulsars (AXMSPs), and finally to binary millisecond pulsars with compact orbit together with UL companions (Podsiadlowski et al. 2002; van Haften et al. 2012; Guo et al. 2024).

12 GPPS discovered pulsars, PSRs J0541+2959g, J1814+0045g, J1830-0106g, J1838+1507g, J1845+0315g, J1847+0342g, J1856+1000g, J1911+1206g, J1919+0126g, J1953+1006g, J2003+3032g and J1953+1844, likely have UL companions. These pulsars are fully recycled. PSRs J1814+0045g and J1953+1006g are black widows exhibiting eclipsing, whose companions have median masses of 0.064 and $0.013 M_\odot$. Eclipse around the egress of PSR J1814+0045g is detected in a short observation, as shown in Figure 9. While the signal is fully eclipsed for J1953+1006g during one observation. Others are black widow candidates. Companions of PSRs J1845+0315g and J1911+1206g are the lightest and are most likely planets.

3.4. Pulsars with main sequence star companions

A small number of pulsars have MS star companions with the median mass $m_{c,med} > 0.5M_\odot$ and orbital period $P_b > 50$ days (Tauris et al. 2012). Some reback systems with $P_b \lesssim 1$ day and $m_c \sim 0.1 - 0.4 M_\odot$ might also have low-mass MS companions that experienced irradiation-induced mass loss.

We have 5 GPPS binary pulsars which likely have MS companions. They are rebacks with MS companions, PSRs J1849+0304g, J1859+0313g, J1919+1502g, J1931+1428g and J1932+2121. They have a companion with a median mass from $0.110M_\odot$ to $0.339M_\odot$ in compact orbits and exhibit eclipses. The eclipses of PSRs J1932+2121, J1849+0304g and J1931+1428g are shown in Figure 9, as revealed by FAST observations. The FAST observation of

⁶ <http://ps1images.stsci.edu/cgi-bin/ps1cutouts>

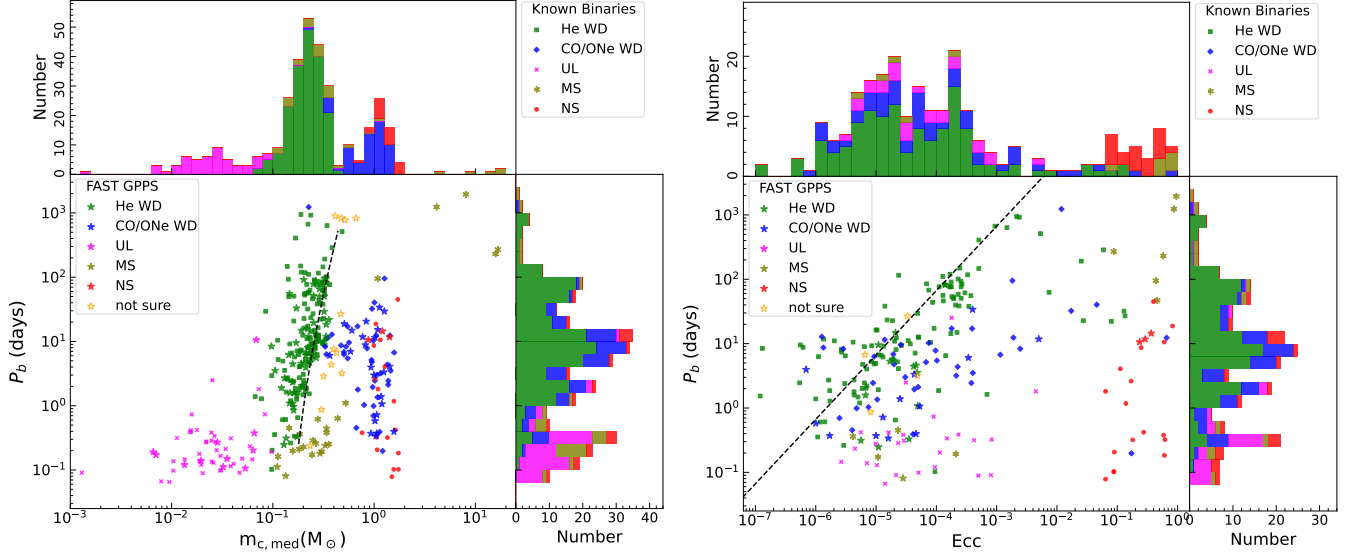


Figure 5. Binary parameters are clustered for various companion types. Binary parameters of previously known pulsars are taken from the ATNF pulsar catalogue (<https://www.atnf.csiro.au/people/pulsar/psrcat/> Manchester et al. 2005), plus the newly discovered binary pulsars by the FAST GPPS survey. In the main panel of the left plot, green squares, blue diamond, red dots, olive asterisks and magenta crosses represent the known He-WD, CO/ONe WD, neutron star (NS), main sequence star (MS) and ultra light (UL) companions, respectively. The binary pulsars reported in this work are represented by stars with colors for various companion types as the known ones and the orange for uncertain companion type. The dashed line is for neutron star - He-WD binaries predicted by Tauris & Savonije (1999). Histograms of the orbital period and companion mass are shown in the right and top panels for the sum of both the known and the new GPPS binaries with different types of companions. In the main panel of the right plot, same data point for the orbital period versus the orbit eccentricity. The dashed line represents the correlation between orbital period and eccentricity for MSP- He-WD systems as proposed by Phinney (1992). Histograms of the orbital period and eccentricity are shown in the right and top panels for the sum of known pulsars and GPPS pulsars.

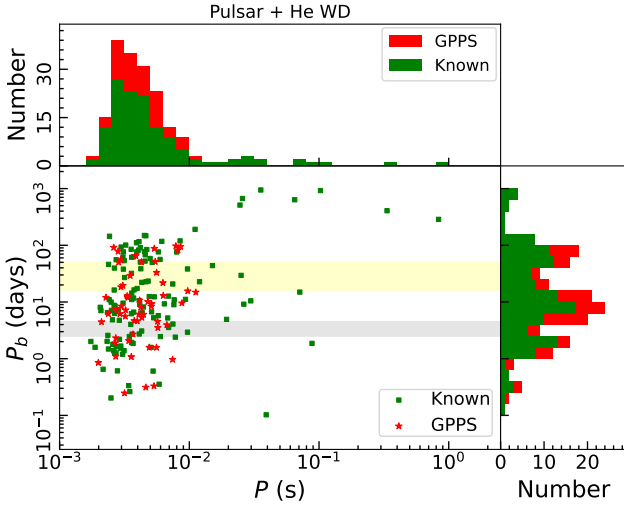


Figure 6. The distribution of pulsar periods and orbit periods for binary pulsars with He-WD companions. In the main panel, green dots represent the 129 known binary pulsars with He-WD companions in the Galactic field, the stars stand for the 56 GPPS pulsars with He-WD companions. The histograms on the top and left show the distributions of pulsar spin period and orbital period.

PSR J1932+2121 exhibits a full eclipse lasting for about 10 minutes that is about 8.6% of the orbital phase. Dur-

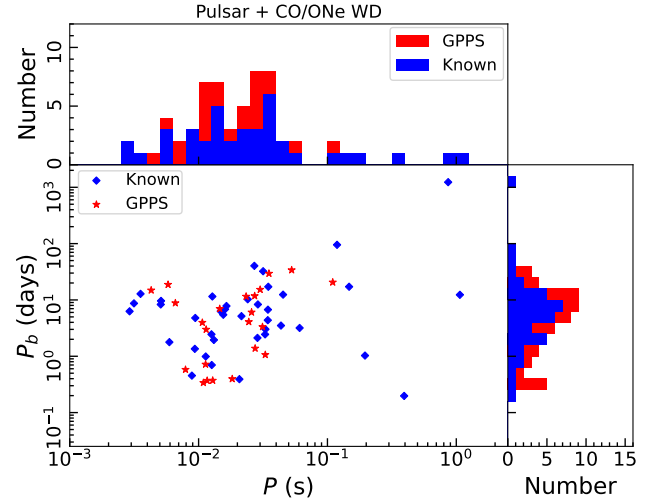


Figure 7. Distribution of pulsar spin periods and orbit periods of binaries with CO/ONe WD companions. There are 39 known systems, plus 23 GPPS binary pulsars with a CO/ONe WD companion.

ing the ingress and egress, pulsar emission is gradually delayed due to the extra DM contributed by the eclipsing material. The egress of eclipse has been also observed for PSR J1849+0304g. The eclipse around ingress is detected in some short observations of PSR 1931+1428g. Eclipses of PSRs

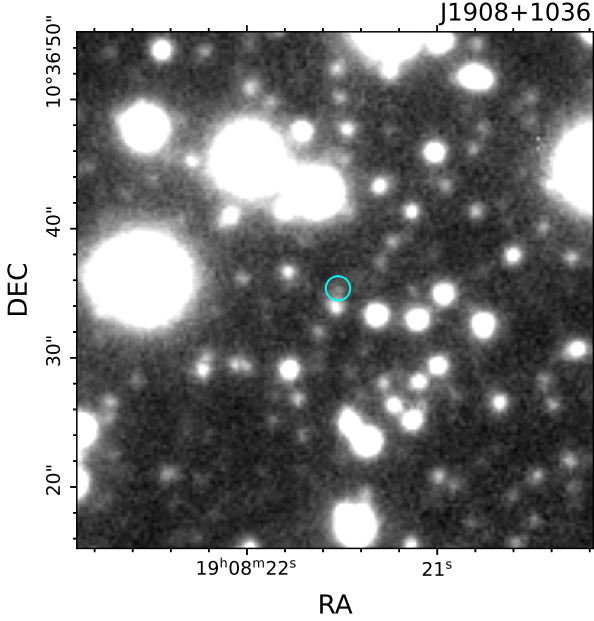


Figure 8. Optical images around the companion of PSR J1908+1036 from Pan-STRARRS1 (Chambers et al. 2016). The cyan circle is centered at the pulsar with a radius of one arcsecond.

J1859+0313g and J1919+1502g result in non-detection of pulsar emission in several observations.

The eclipses can be observed at multiple wavelengths and are desired for careful investigation to understand the outflowing material from the companion stars (e.g. Podsiadlowski 1991), the companion properties and the binary orbit (e.g. Main et al. 2018; Li et al. 2019; Du et al. 2023), which is hard to include in this paper.

3.5. Pulsars with NS companions

The double neutron star binary systems are generally formed from HMXBs through the Case BB RLO following a CE phase, which leads to mild or marginal recycling for the first-born NSs (Tauris et al. 2017). As summarized by Su et al. (2024), there have been about 28 double neutron star systems, 23 DNS in the Galactic field (including 5 DNS candidates: PSRs J1753–2240, J1755–2550, J1759+5036, J1906+0746, and J2150+3427) with an orbital period in the range from 0.078 to 50 days and an eccentricity in the range from 0.064 to 0.828 (Tauris et al. 2012).

In the discovery of the FAST GPPS survey, three binary pulsars, PSRs J0528+3529, J1844-0128 and J1901+0658, are most likely in DNS systems. PSR J1901+0658 is the first GPPS discovered pulsar, and was reported in Su et al. (2024).

PSR J0528+3529 has a spin period of 78.2 ms and a period derivative of $7.36 \times 10^{-19} \text{ s s}^{-1}$. It is in an elliptic orbit with a period of 11.73 days and an eccentricity of 0.29. The ephemeris is presented in Table 4. Its companion is estimated to have a median mass of $1.42 M_{\odot}$. The relatively large companion mass together with the large eccentricity indicates that

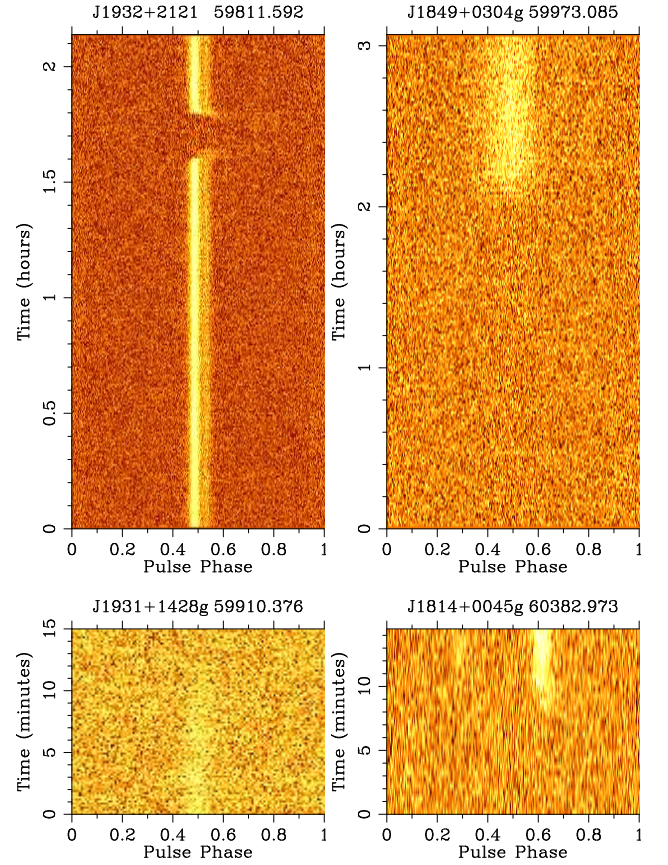


Figure 9. Eclipses of four binary pulsars. PSRs J1932+2121 and J1849+0304g are observed for 2.1 and 3.1 hours, PSRs J1931+1428g and J1814+0045g are observed for 15 minutes each.

the companion is most likely a neutron star. Our timing observations demonstrate that its periastron advances with $\dot{\omega}$ of $0.0073(2) \text{ deg/yr}$ (see Table 4). According to general relativity, the rate of advance of the periastron is described by (Blandford & Teukolsky 1976; Damour & Deruelle 1985),

$$\dot{\omega} = 3T_{\odot}^{2/3} \left(\frac{P_b}{2\pi} \right)^{-5/3} \frac{1}{1 - e^2} (m_p + m_c)^{2/3}. \quad (2)$$

With which, total mass of the system is estimated to be $2.90(12) M_{\odot}$. The possible mass spaces for both the pulsar and its neutron star companion is shown in Figure 10.

PSR J1844-0128 has a spin period of 29.1 ms, and is in an eccentric orbit with a period of 10.6 days and an eccentricity of 0.237. Its companion is estimated to have a median mass of $0.87 M_{\odot}$, as listed in Table 3. Its periastron advance is marginally detect with $\dot{\omega}$ of $0.0059(18) \text{ deg/yr}$, which indicates a total mass of $1.7(8) M_{\odot}$.

3.6. Pulsars with a helium MS companion

PSR J1928+1815 is in a compact circular orbit with a companion with a median mass of $1.395 M_{\odot}$ and shows the eclipse near the conjunction phase. Yang et al (2024a) suggested the companion to be a He main-sequence star.

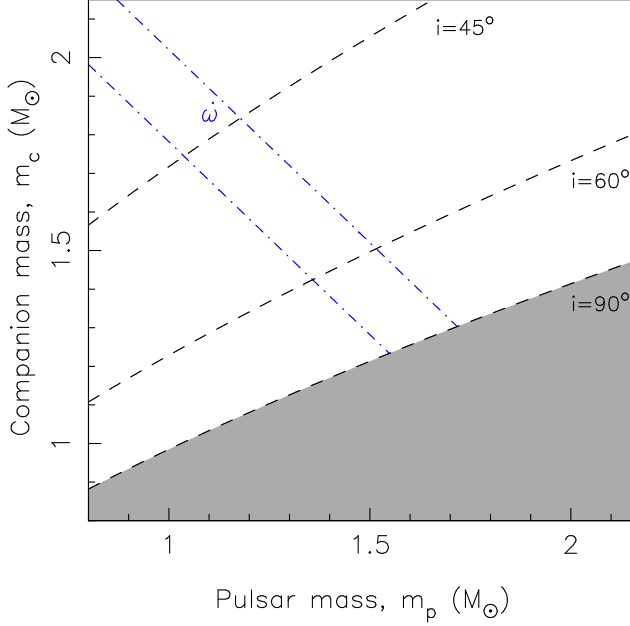


Figure 10. Mass-mass diagram of the double neutron star system PSR J0528+3529. The gray area represents the excluded parameter spaces from its mass function, with the boundary defined by an inclination angle of $i = 90^\circ$. The area between two dash-dotted blue lines is the possible parameter space, as constrained by the measured $\dot{\omega}$ within $\pm 1\sigma$.

3.7. Pulsars with undetermined companions

The companion nature of a binary system discussed above is inferred based on previous knowledge. However there are too many evolution channels, each with very uncertain parameters. There are some ambiguous parameter space between the NS He-WD binary and the NS CO-WD binary, or between the NS He-WD binary and the NS-MS binary, or between the NS CO-WD binary and the DNS binary. Such an ambiguity is mainly caused by the unknown orbital inclination angle and the lack of companion observations at other wave bands. Among newly discovered binary pulsars by the FAST GPPS survey, 11 pulsars may have a companion of either a He-WD or CO-WD, and one pulsars have a companion of either He-WD or MS star.

PSRs J1838+0028g, J1842+0407g, J1857+0642, J1908+0949, J1917+1259 and J1943+2206 are fully recycled millisecond pulsars in orbits with periods of 3-27 days. The median masses of companion are in the range of 0.32 to $0.48 M_\odot$. Such systems are typical descendants from the IMXB Case A evolution channel, and their companions are either CO-WDs or He-WDs (Tauris 2011).

PSRs J1900+0213g, J1910+0423g, J1917+1046g and J1923+2022g are typical descendants of LMXBs but in orbit with periods as long as almost 900 days. It is then difficult to assess the companion to be a He-WD or CO-WD according to Tauris & Savonije (1999). PSR J1952+2837 has a companion mass large and beyond that predicted by the P_b versus m_c relationship for the typical He-WDs. Moreover,

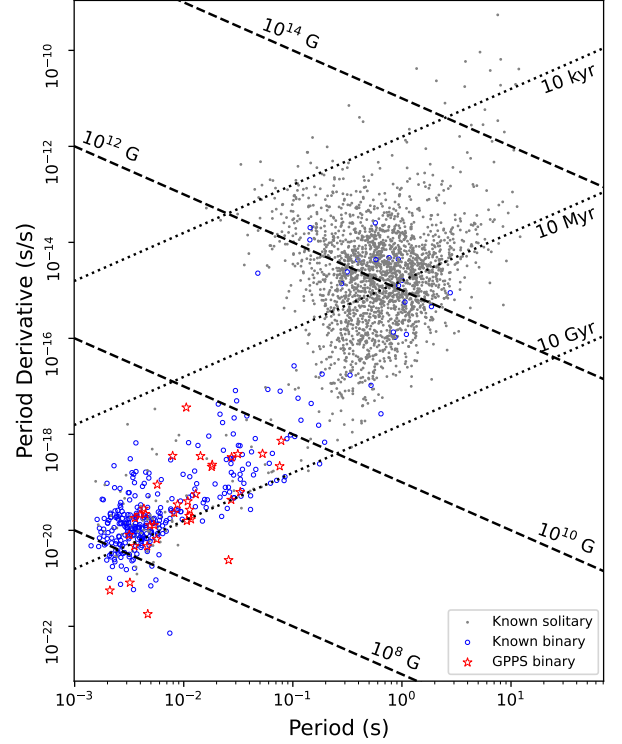


Figure 11. Binary pulsars in the period versus period derivative diagram. Gray dots represent solidly single pulsars listed in the ATNF pulsar catalogue (Manchester et al. 2005). Binary pulsars are indicated by circles. The newly discovered 36 binary pulsars by the GPPS survey which have timing solutions already are indicated by red stars. Dashed and dotted lines represent constant surface magnetic field and characteristic age, respectively.

unlike typical descendants of LMXBs, PSR J1952+2837 is mildly recycled with a spin period of 18 ms which probably evolve from an IMXB. The median companion mass is $0.30 M_\odot$, which cannot be a CO-WD unless its orbital inclination is sufficiently low. But if the companion is a He-WD, the formation channel for such a system is unclear.

PSRs J1857-0125g has an orbital period of 0.24 days and a median companion mass of $m_{c,med} = 0.23 M_\odot$. Such a low-mass companion might be a He-WD or an MS exhibiting as redback systems with feedback from the neutron star (Chen et al. 2013; Strader et al. 2019). Further observations are desired to determine the companion nature by uncovering the possible pulsar eclipses and orbital period variations.

4. CONCLUSIONS AND DISCUSSION

In this work, we report 112 binary pulsars discovered by the FAST GPPS survey. We have got the timing solutions of 36 binary pulsars measured, as indicated in the distribution in the $P - \dot{P}$ diagram in Figure 11. In addition to the timing solutions for 9 pulsars published previously, we present the measured and derived parameters for 27 binary pulsars with phase-coherent timing solutions. For the other 76 pul-

Table 7. Kinematic corrections of \dot{P} and relevant parameters for 4 pulsars with proper motion measurement.

Pulsar	μ_T (mas yr ⁻¹)	\dot{P} (10 ⁻²¹ s s ⁻¹)	\dot{P}_S (10 ⁻²¹ s s ⁻¹)	\dot{P}_G (10 ⁻²¹ s s ⁻¹)	\dot{P}_I (10 ⁻²¹ s s ⁻¹)	$B_{\text{surf,c}}$ (10 ⁸ Gs)	τ_c (Gyr)	\dot{E}_c (10 ³³ erg s ⁻¹)
(1)	(2)	(3)	(4)	(5)	(6)	(7)	(8)	(9)
J1857+0642	5.9(9)	4.69	0.30	0.03	4.36	1.26	12.80	3.91
J1903+0839	5.0(9)	4.67	1.49	-1.78	4.96	1.53	14.74	1.98
J1904+0553	8.3(13)	12.75	3.65	-0.94	10.04	2.25	7.72	3.36
J1908+1036	12.0(22)	15.73	2.51	-0.03	13.25	3.81	12.75	0.43

Notes: μ_T : total proper motion, \dot{P}_S : Shklovskii effect, \dot{P}_G : Galactic acceleration, \dot{P}_I : intrinsic period derivative, $B_{\text{surf,c}}$: corrected surface magnetic field, τ_c : corrected age, \dot{E}_c : corrected energy loss rate.

sars, we have got the best-fitted Keplerian parameters of the binary orbits based on several FAST observations. Most of the binary systems need to be further timed in the future, so that precise spin and orbital parameters of the systems with preliminary Keplerian parameters can be obtained. The PK parameters of the relativistic systems can be measured and improved. For example, the possible Shapiro delay in tight systems requires long term monitoring with good cadence and observation sensitivity.

With currently available measurements, we see that the pulsar binary systems we discovered in the GPPS survey have a broad range of spin periods, orbital periods and eccentricity. Among 112 pulsars, 97 of them have spin period $P < 30$ ms; 30 GPPS binaries have orbital periods shorter than one day and two of them shorter than 0.1 day. The shortest is 53 minutes for the black widow pulsar PSR J1953+1844 (Pan et al. 2023). The observed \dot{P} of PSR J1943+2206 is the smallest among all the binary pulsars reported in this work. The inferred surface magnetic field strength is only 2.95×10^7 G.

Most of these binary pulsars have nearly circular orbits with $e \ll 0.001$, with He- or CO/ONe-WD companions in general. We noticed that 3 pulsars, PSRs J0528+3529, J1901+0658, J1844–0127g, have orbital eccentricities $e > 0.01$. Because of the large companion masses, they are very likely double NS systems, or NS-WD systems in which the NS formed after the massive WD, or a NS-MS system with a newly born NS. For evolved DNS or NS-WD systems, the large eccentricity indicates that the second formed object is most likely a compact NS if a significant eccentricity remains from the second supernova explosion (Tauris & van den Heuvel 2023).

Among these binaries discovered by the FAST GPPS survey, 56 pulsars rotate with He-WD companions in the orbit, 23 pulsars with a CO/ONe-WD companion, 11 pulsars with an UL companion, 5 with a MS companion, 3 pulsars with a NS companion and one with a He star as companion. We have 12 pulsars with companion of unknown natures. Combining these GPPS binaries with those known ones, we get the largest binary sample in the Galactic field. The He-WD, CO/ONe WD, UL, MS and NS systems have fractions of 43.4%, 14.6%, 12.4%, 6.3% and 4.7%, in total.

For these pulsars with timing solutions, we obtained polarization pulse profiles by combining multiple FAST observations. The Geometry parameters of the emission regions have been derived from the polarization angle curves fitted by the RMV model. Optical counterpart is found for the companion of PSR J1908+1036 from the Pan-STARRS survey. The non-detection reveals that He-WD companions are generally cool and old. Post-Keplerian parameter $\dot{\omega}$ has been measured for the double neutron star system PSR J0528+3529, from which the total mass of the system is estimated to be $2.90(12)M_{\odot}$.

For very nearby pulsars, it should be noted that the observed pulsar spin down rate comprises its intrinsic term \dot{P}_I plus the contributions from the Shklovskii effect \dot{P}_S and the Galactic acceleration \dot{P}_G , in the form of

$$\dot{P} = \dot{P}_I + \dot{P}_S + \dot{P}_G. \quad (3)$$

The Shklovskii effect results from the increase of projected distance between pulsar and solar system barycenter when a pulsar moves, which leads to the increase of pulse period (Backer & Hellings 1986). The Shklovskii term, \dot{P}_S , as indicated in column (4) in Table 7, contributes 32% of the measured \dot{P} for PSR J1903+0837. In a differential Galactic potential, the acceleration between a pulsar and the solar system barycenter, i.e., the Galactic acceleration term, can be found from Nice & Taylor (1995). We list the influences of gravitational acceleration \dot{P}_G listed in column (5) of Table 7. They are generally negative except for PSR J1857+0642. Its influence on period derivatives is more than 18% for PSR J1903+0839. Both the Shklovskii effect and the Galactic acceleration term can not be neglected in calculating the intrinsic \dot{P}_I . With \dot{P}_I , the surface magnetic field, characteristic age and spin-down energy loss rate are reestimated, as listed in columns (7)-(9) of Table 7.

FAST is a Chinese national mega-science facility built and operated by the National Astronomical Observatories, Chinese Academy of Sciences. P. F. Wang is supported by the National Natural Science Foundation of China (No. 12133004), the National SKA program of China (No. 2020SKA0120200) and the National Key R&D Program of China (No. 2021YFA1600401 and 2021YFA1600400). J. L. Han is supported by the National Natural Science Foundation of China (No. 11988101 and 11833009).

REFERENCES

- Alam, M. F., Arzoumanian, Z., Baker, P. T., et al. 2021, *ApJS*, 252, 5, doi: [10.3847/1538-4365/abc6a1](https://doi.org/10.3847/1538-4365/abc6a1)
- Alpar, M. A., Cheng, A. F., Ruderman, M. A., & Shaham, J. 1982, *Nature*, 300, 728, doi: [10.1038/300728a0](https://doi.org/10.1038/300728a0)
- Antoniadis, J. 2014, *ApJL*, 797, L24, doi: [10.1088/2041-8205/797/2/L24](https://doi.org/10.1088/2041-8205/797/2/L24)
- Antoniadis, J., Tauris, T. M., Özel, F., et al. 2016, arXiv e-prints, arXiv:1605.01665, doi: [10.48550/arXiv.1605.01665](https://doi.org/10.48550/arXiv.1605.01665)
- Antoniadis, J., Freire, P. C. C., Wex, N., et al. 2013, *Science*, 340, 448, doi: [10.1126/science.1233232](https://doi.org/10.1126/science.1233232)
- Backer, D. C., & Hellings, R. W. 1986, *ARA&A*, 24, 537, doi: [10.1146/annurev.aa.24.090186.002541](https://doi.org/10.1146/annurev.aa.24.090186.002541)
- Bhattacharya, D., & van den Heuvel, E. P. J. 1991, *PhR*, 203, 1, doi: [10.1016/0370-1573\(91\)90064-S](https://doi.org/10.1016/0370-1573(91)90064-S)
- Blandford, R., & Teukolsky, S. A. 1976, *ApJ*, 205, 580, doi: [10.1086/154315](https://doi.org/10.1086/154315)
- Cameron, A. D., Champion, D. J., Kramer, M., et al. 2018, *MNRAS*, 475, L57, doi: [10.1093/mnras/sly003](https://doi.org/10.1093/mnras/sly003)
- Chambers, K. C., Magnier, E. A., Metcalfe, N., et al. 2016, arXiv e-prints, arXiv:1612.05560, doi: [10.48550/arXiv.1612.05560](https://doi.org/10.48550/arXiv.1612.05560)
- Chen, H.-L., Chen, X., Tauris, T. M., & Han, Z. 2013, *ApJ*, 775, 27, doi: [10.1088/0004-637X/775/1/27](https://doi.org/10.1088/0004-637X/775/1/27)
- Chen, H.-L., Tauris, T. M., Han, Z., & Chen, X. 2021, *MNRAS*, 503, 3540, doi: [10.1093/mnras/stab670](https://doi.org/10.1093/mnras/stab670)
- Corbet, R. H. D. 1984, *A&A*, 141, 91
- Cordes, J. M., & Lazio, T. J. W. 2002, arXiv e-prints, astro, doi: [10.48550/arXiv.astro-ph/0207156](https://doi.org/10.48550/arXiv.astro-ph/0207156)
- Damour, T., & Deruelle, N. 1985, *Annales de L'Institut Henri Poincare Section (A) Physique Theorique*, 43, 107
- Demorest, P. B., Pennucci, T., Ransom, S. M., Roberts, M. S. E., & Hessels, J. W. T. 2010, *Nature*, 467, 1081, doi: [10.1038/nature09466](https://doi.org/10.1038/nature09466)
- Deneva, J. S., Ray, P. S., Camilo, F., et al. 2021, *ApJ*, 909, 6, doi: [10.3847/1538-4357/abd7a1](https://doi.org/10.3847/1538-4357/abd7a1)
- Du, Z.-X., Yu, Y.-W., Chen, A. M., et al. 2023, *Research in Astronomy and Astrophysics*, 23, 125024, doi: [10.1088/1674-4527/ad034b](https://doi.org/10.1088/1674-4527/ad034b)
- Freire, P. C., Kramer, M., & Lyne, A. G. 2001, *MNRAS*, 322, 885, doi: [10.1046/j.1365-8711.2001.04200.x](https://doi.org/10.1046/j.1365-8711.2001.04200.x)
- Freire, P. C. C., & Ridolfi, A. 2018, *MNRAS*, 476, 4794, doi: [10.1093/mnras/sty524](https://doi.org/10.1093/mnras/sty524)
- Freire, P. C. C., Bassa, C. G., Wex, N., et al. 2011, *MNRAS*, 412, 2763, doi: [10.1111/j.1365-2966.2010.18109.x](https://doi.org/10.1111/j.1365-2966.2010.18109.x)
- Freire, P. C. C., Wex, N., Esposito-Farèse, G., et al. 2012, *MNRAS*, 423, 3328, doi: [10.1111/j.1365-2966.2012.21253.x](https://doi.org/10.1111/j.1365-2966.2012.21253.x)
- Guo, Y., Wang, B., & Li, X. 2024, *MNRAS*, 527, 7394, doi: [10.1093/mnras/stad3613](https://doi.org/10.1093/mnras/stad3613)
- Han, J. L., Wang, C., Wang, P. F., et al. 2021, *Research in Astronomy and Astrophysics*, 21, 107, doi: [10.1088/1674-4527/21/5/107](https://doi.org/10.1088/1674-4527/21/5/107)
- Han, J. L., Zhou, D. J., Wang, C., et al. 2024, arXiv, arXiv:2411.15961, doi: [10.48550/arXiv.2411.15961](https://doi.org/10.48550/arXiv.2411.15961)
- Hobbs, G., Guo, L., Caballero, R. N., et al. 2020, *MNRAS*, 491, 5951, doi: [10.1093/mnras/stz3071](https://doi.org/10.1093/mnras/stz3071)
- Hobbs, G. B., Edwards, R. T., & Manchester, R. N. 2006, *MNRAS*, 369, 655, doi: [10.1111/j.1365-2966.2006.10302.x](https://doi.org/10.1111/j.1365-2966.2006.10302.x)
- Hotan, A. W., van Straten, W., & Manchester, R. N. 2004, *PASA*, 21, 302, doi: [10.1071/AS04022](https://doi.org/10.1071/AS04022)
- Hu, H., Kramer, M., Wex, N., Champion, D. J., & Kehl, M. S. 2020, *MNRAS*, 497, 3118, doi: [10.1093/mnras/staa2107](https://doi.org/10.1093/mnras/staa2107)
- Hui, C. Y., Wu, K., Han, Q., Kong, A. K. H., & Tam, P. H. T. 2018, *ApJ*, 864, 30, doi: [10.3847/1538-4357/aad5ec](https://doi.org/10.3847/1538-4357/aad5ec)
- Istrate, A. G., Tauris, T. M., & Langer, N. 2014, *A&A*, 571, A45, doi: [10.1051/0004-6361/201424680](https://doi.org/10.1051/0004-6361/201424680)
- Ivanova, N., Justham, S., Chen, X., et al. 2013, *A&A Rv*, 21, 59, doi: [10.1007/s00159-013-0059-2](https://doi.org/10.1007/s00159-013-0059-2)
- Jiang, P., Tang, N.-Y., Hou, L.-G., et al. 2020, *Research in Astronomy and Astrophysics*, 20, 064, doi: [10.1088/1674-4527/20/5/64](https://doi.org/10.1088/1674-4527/20/5/64)
- Kaspi, V. M., Lyne, A. G., Manchester, R. N., et al. 2000, *ApJ*, 543, 321, doi: [10.1086/317103](https://doi.org/10.1086/317103)
- Koester, D., & Reimers, D. 2000, *A&A*, 364, L66
- Kramer, M., Stairs, I. H., Manchester, R. N., et al. 2006, *Science*, 314, 97, doi: [10.1126/science.1132305](https://doi.org/10.1126/science.1132305)
- Kramer, M., Stairs, I. H., Venkatraman Krishnan, V., et al. 2021, *MNRAS*, 504, 2094, doi: [10.1093/mnras/stab375](https://doi.org/10.1093/mnras/stab375)
- Lange, C., Camilo, F., Wex, N., et al. 2001, *MNRAS*, 326, 274, doi: [10.1046/j.1365-8711.2001.04606.x](https://doi.org/10.1046/j.1365-8711.2001.04606.x)
- Lentati, L., Taylor, S. R., Mingarelli, C. M. F., et al. 2015, *MNRAS*, 453, 2576, doi: [10.1093/mnras/stv1538](https://doi.org/10.1093/mnras/stv1538)
- Li, D., Lin, F. X., Main, R., et al. 2019, *MNRAS*, 484, 5723, doi: [10.1093/mnras/stz374](https://doi.org/10.1093/mnras/stz374)
- Main, R., Yang, I. S., Chan, V., et al. 2018, *Nature*, 557, 522, doi: [10.1038/s41586-018-0133-z](https://doi.org/10.1038/s41586-018-0133-z)
- Manchester, R. N., Hobbs, G. B., Teoh, A., & Hobbs, M. 2005, *AJ*, 129, 1993, doi: [10.1086/428488](https://doi.org/10.1086/428488)
- Miao, C. C., Zhu, W. W., Li, D., et al. 2023, *MNRAS*, 518, 1672, doi: [10.1093/mnras/stac1305](https://doi.org/10.1093/mnras/stac1305)
- Nan, R. 2006, *Science in China: Physics, Mechanics and Astronomy*, 49, 129, doi: [10.1007/s11433-006-0129-9](https://doi.org/10.1007/s11433-006-0129-9)
- Nan, R., Li, D., Jin, C., et al. 2011, *International Journal of Modern Physics D*, 20, 989, doi: [10.1142/S0218271811019335](https://doi.org/10.1142/S0218271811019335)
- Nice, D. J., & Taylor, J. H. 1995, *ApJ*, 441, 429, doi: [10.1086/175367](https://doi.org/10.1086/175367)
- Özel, F., & Freire, P. 2016, *ARA&A*, 54, 401, doi: [10.1146/annurev-astro-081915-023322](https://doi.org/10.1146/annurev-astro-081915-023322)

- Pan, Z., Lu, J. G., Jiang, P., et al. 2023, *Nature*, 620, 961, doi: [10.1038/s41586-023-06308-w](https://doi.org/10.1038/s41586-023-06308-w)
- Park, R. S., Folkner, W. M., Williams, J. G., & Boggs, D. H. 2021, *AJ*, 161, 105, doi: [10.3847/1538-3881/abd414](https://doi.org/10.3847/1538-3881/abd414)
- Phinney, E. S. 1992, *Philosophical Transactions of the Royal Society of London Series A*, 341, 39, doi: [10.1098/rsta.1992.0084](https://doi.org/10.1098/rsta.1992.0084)
- Phinney, E. S., & Kulkarni, S. R. 1994, *ARA&A*, 32, 591, doi: [10.1146/annurev.aa.32.090194.003111](https://doi.org/10.1146/annurev.aa.32.090194.003111)
- Podsiadlowski, P. 1991, *Nature*, 350, 136, doi: [10.1038/350136a0](https://doi.org/10.1038/350136a0)
- Podsiadlowski, P., Rappaport, S., & Pfahl, E. D. 2002, *ApJ*, 565, 1107, doi: [10.1086/324686](https://doi.org/10.1086/324686)
- Pylyser, E., & Savonije, G. J. 1988, *A&A*, 191, 57
- Radhakrishnan, V., & Cooke, D. J. 1969, *Astrophys. Lett.*, 3, 225
- Reardon, D. J., Shannon, R. M., Cameron, A. D., et al. 2021, *MNRAS*, 507, 2137, doi: [10.1093/mnras/stab1990](https://doi.org/10.1093/mnras/stab1990)
- Refsdal, S., & Weigert, A. 1971, *A&A*, 13, 367
- Roberts, M. S. E. 2013, in *Neutron Stars and Pulsars: Challenges and Opportunities after 80 years*, ed. J. van Leeuwen, Vol. 291, 127–132, doi: [10.1017/S174392131202337X](https://doi.org/10.1017/S174392131202337X)
- Strader, J., Chomiuk, L., Cheung, C. C., et al. 2015, *ApJL*, 804, L12, doi: [10.1088/2041-8205/804/1/L12](https://doi.org/10.1088/2041-8205/804/1/L12)
- Strader, J., Swihart, S., Chomiuk, L., et al. 2019, *ApJ*, 872, 42, doi: [10.3847/1538-4357/aafbaa](https://doi.org/10.3847/1538-4357/aafbaa)
- Su, W. Q., Han, J. L., Yang, Z. L., et al. 2024, *MNRAS*, 530, 1506, doi: [10.1093/mnras/stae888](https://doi.org/10.1093/mnras/stae888)
- Taam, R. E., King, A. R., & Ritter, H. 2000, *ApJ*, 541, 329, doi: [10.1086/309392](https://doi.org/10.1086/309392)
- Tauris, T. M. 1996, *A&A*, 315, 453
- Tauris, T. M. 2011, in *Astronomical Society of the Pacific Conference Series*, Vol. 447, *Evolution of Compact Binaries*, ed. L. Schmidtbreick, M. R. Schreiber, & C. Tappert, 285, doi: [10.48550/arXiv.1106.0897](https://doi.org/10.48550/arXiv.1106.0897)
- Tauris, T. M., Langer, N., & Kramer, M. 2011, *MNRAS*, 416, 2130, doi: [10.1111/j.1365-2966.2011.19189.x](https://doi.org/10.1111/j.1365-2966.2011.19189.x)
- . 2012, *MNRAS*, 425, 1601, doi: [10.1111/j.1365-2966.2012.21446.x](https://doi.org/10.1111/j.1365-2966.2012.21446.x)
- Tauris, T. M., & Savonije, G. J. 1999, *A&A*, 350, 928, <https://arxiv.org/abs/astro-ph/9909147>
- Tauris, T. M., & van den Heuvel, E. P. J. 2006, in *Compact stellar X-ray sources*, Vol. 39 (Cambridge University Press), 623–665, doi: [10.48550/arXiv.astro-ph/0303456](https://doi.org/10.48550/arXiv.astro-ph/0303456)
- Tauris, T. M., & van den Heuvel, E. P. J. 2023, *Physics of Binary Star Evolution. From Stars to X-ray Binaries and Gravitational Wave Sources* (Princeton University Press), doi: [10.48550/arXiv.2305.09388](https://doi.org/10.48550/arXiv.2305.09388)
- Tauris, T. M., Kramer, M., Freire, P. C. C., et al. 2017, *ApJ*, 846, 170, doi: [10.3847/1538-4357/aa7e89](https://doi.org/10.3847/1538-4357/aa7e89)
- van Haaften, L. M., Nelemans, G., Voss, R., Wood, M. A., & Kuijpers, J. 2012, *A&A*, 537, A104, doi: [10.1051/0004-6361/201117880](https://doi.org/10.1051/0004-6361/201117880)
- van Straten, W., & Bailes, M. 2011, *PASA*, 28, 1, doi: [10.1071/AS10021](https://doi.org/10.1071/AS10021)
- Venkatraman Krishnan, V., Bailes, M., van Straten, W., et al. 2020, *Science*, 367, 577, doi: [10.1126/science.aax7007](https://doi.org/10.1126/science.aax7007)
- Voisin, G., Cognard, I., Freire, P. C. C., et al. 2020, *A&A*, 638, A24, doi: [10.1051/0004-6361/202038104](https://doi.org/10.1051/0004-6361/202038104)
- Wang, P. F., Han, J. L., Xu, J., et al. 2023, *Research in Astronomy and Astrophysics*, 23, 104002, doi: [10.1088/1674-4527/acea1f](https://doi.org/10.1088/1674-4527/acea1f)
- Webbink, R. F., Rappaport, S., & Savonije, G. J. 1983, *ApJ*, 270, 678, doi: [10.1086/161159](https://doi.org/10.1086/161159)
- Weisberg, J. M., & Huang, Y. 2016, *ApJ*, 829, 55, doi: [10.3847/0004-637X/829/1/55](https://doi.org/10.3847/0004-637X/829/1/55)
- Weisberg, J. M., & Taylor, J. H. 1984, *PhRvL*, 52, 1348, doi: [10.1103/PhysRevLett.52.1348](https://doi.org/10.1103/PhysRevLett.52.1348)
- Xu, H., Chen, S., Guo, Y., et al. 2023, *Research in Astronomy and Astrophysics*, 23, 075024, doi: [10.1088/1674-4527/acdfa5](https://doi.org/10.1088/1674-4527/acdfa5)
- Yang, Z. L., Han, J. L., Jing, W. C., & Su, W. Q. 2023, *ApJL*, 956, L39, doi: [10.3847/2041-8213/acfe6e](https://doi.org/10.3847/2041-8213/acfe6e)
- Yang, Z. L., Han, J. L., Wang, T., et al. 2024a, *Research in Astronomy and Astrophysics*, 24
- Yang, Z. L., Han, J. L., Zhou, D. J., et al. 2024b, *Science*, in press
- Yao, J. M., Manchester, R. N., & Wang, N. 2017, *ApJ*, 835, 29, doi: [10.3847/1538-4357/835/1/29](https://doi.org/10.3847/1538-4357/835/1/29)

APPENDIX

LARGE FIGURES AND TABLES FOR BINARY PULSARS

In the main text of this paper, we give only one example of timing solution. Here we present the timing solutions of 27 binary pulsars. Their ephemerides are listed in Table A1. All ephemerides obtained here are based on the DE440 solar system ephemeris model, the Barycentric Dynamical Time (TDB) units, and TT(TAI) clock. The ephemeris items include standard pulsar name defined by accurate position, the temperate name and the GPPS discovery number, the MJD range and the span for FAST observation data and number of TOAs. Measured quantities include: right ascension (RA) in hh:mm:ss.ss, declination (DEC) in +/-dd:mm:ss.s, dispersion measure (DM) in cm^{-3} pc, pulsar rotation frequency ν in Hz, first derivative of pulsar rotation frequency $\dot{\nu}$ in 10^{-16} Hz per second, proper motion in right ascension $\mu_\alpha \cos \delta$ in milli-arc-second (mas) per year (if measured), proper motion in declination μ_δ in milli-arc-second (mas) per year (if measured), the timing residue in microsecond (μs); timing residual scaling factor EFAC; timing residual quadratic adding factor EQUAD; Reduced χ^2 of model-fitting. Binary parameters include orbital period P_b in days, projected semi-major axis of pulsar's orbit x in light-years, the time of passing through periastron T_0 (if measured), the longitude of periastron ω (if measured), time of ascending node T_{asc} in MJD, first and second Laplace parameters e_1 and e_2 . (3) Derived quantities include: the Galactic longitude l in degree, the Galactic latitude b in degree, distance estimates D_{YMW} and D_{NE2001} by using the Galactic electron density distribution models YMW17 (Yao et al. 2017) and NE2001 (Cordes & Lazio 2002) in kpc, the spin period of a pulsar P in second, the derivative of the spin period \dot{P} in *secondpersecond*, characteristic age τ in Gyr, surface magnetic field strengt B_{surf} in 10^8G , and the orbital eccentricity e (if measured).

Timing residuals of 27 binary pulsars are shown in Figure A1. The left panels are for the residuals along the observation epochs, and the right panels for residuals versus the orbital phase.

For these pulsars with timing solution, we can add all FAST polarization measurements and get their polarization profiles, as shown in Figure A2. We tried to fit the polarization angle curves with the rotating vector model (Radhakrishnan & Cooke 1969) for 5 pulsars, PSRs J1840+0012, J1857+0642, J1916+0740, J1930+1403 and J1946+0904.

For 76 binary pulsars without timing solutions, the measurements of barycentric periods are plotted across the orbit phase in Figure A3, together with the currently best-fitting preliminary Keplerian model. These data are the base for further follow-up observations.

Table A1. Phase-coherent timing solutions of 27 binary pulsars.

Pulsar name	J0528+3529	J0622+0339	J1840+0012	J1844-0128	J1844+0028
GPPS number	gpps0537	gpps0388	gpps0146	gpps0555	gpps0109
MJD range	59930 – 60625	59645 – 60484	59188 – 60062	59321 – 60604	58852 – 60138
Data Span (yr)	1.9	2.3	2.4	3.5	3.5
Number of TOAs	23	106	78	59	52
Ref. epoch (MJD)	60000	60000	59500	60000	59500
Measured quantities					
RA (hh:mm:ss)	05:28:28.7978(1)	06:22:19.4862(2)	18:40:49.2066(1)	18:44:20.995(2)	18:44:37.3595(2)
DEC(dd:mm:ss)	+35:29:36.81(3)	+03:39:42.882(11)	+00:12:30.007(4)	-01:28:25.77(5)	+00:28:12.582(8)
DM (cm ⁻³ pc)	111.837	79.4186(10)	100.840(3)	368.179	181.094
ν (Hz)	12.78221930378(2)	114.00514689571(2)	187.30193394493(5)	34.31188264149(10)	280.05934666221(6)
$\dot{\nu}$ (10 ⁻¹⁶ Hz s ⁻¹)	-1.202(4)	-4.51(5)	-4.52(2)	-0.36(4)	-14.17(3)
Residual (μ s)	6.037	5.244	12.660	154.288	17.199
EFAC	0.77	1.0	1.0	0.85	1.0
EQUAD	0.0	0.0	0.0	0.0	0.0
Reduced χ^2	0.99	1.10	1.07	1.07	1.11
Binary parameters					
Binary model	DD	ELL1	ELL1	DD	ELL1
P_b (d)	11.7261813(4)	9.54626602(4)	0.3285676513(13)	10.6003185(14)	1.078895359(3)
x (lt-s)	31.43468(2)	4.891818(7)	0.528904(3)	20.96779(6)	1.059555(5)
T_{asc} (MJD)	-	60003.173741(4)	59188.3036687(12)	-	59570.1860995(13)
ϵ_1 (10 ⁻⁵)	-	-0.69(10)	-2.2(21)	-	1.2(11)
ϵ_2 (10 ⁻⁵)	-	-0.80(40)	2.7(29)	-	-4.7(27)
T_0 (MJD)	59994.190822(8)	-	-	60001.62635(7)	-
e	0.2901088(10)	-	-	0.234949(5)	-
ω (deg)	184.9436(2)	-	-	255.699(3)	-
$\dot{\omega}$ (deg/yr)	0.0072(3)	-	-	0.0059(18)	-
Derived quantities					
l (deg)	172.52387(3)	206.334480(3)	31.9063976(3)	-	32.573422(3)
b (deg)	0.46700(2)	-4.783911(2)	2.4573192(4)	-	1.7307459(3)
D_{YMW} (kpc)	1.933	1.786	3.521	-	4.565
D_{NE2001} (kpc)	2.950	2.585	2.946	-	5.015
P (ms)	78.23367572047(12)	8.771533805528(2)	5.3389731698873(15)	29.14442236961(9)	3.5706717591045(8)
\dot{P} (10 ⁻²¹ s s ⁻¹)	736(2)	34.7(3)	12.89(4)	31(4)	18.07(4)
τ (Gyr)	1.686	4.008	6.569	15.001	3.133
B_{surf} (10 ⁸ G)	76.762	5.583	2.654	9.588	2.571
e (10 ⁻⁵)	-	1.06(26)	3.5(26)	-	4.9(26)

Table A1. – continued –

Pulsar name	J1845+0201	J1857+0642	J1903+0839	J1904+0553	J1905+0649
GPPS number	gpps0547	gpps0236	gpps0100	gpps0039	gpps0229
MJD range	59768 – 60518	59425 – 60409	58936 – 60402	58898 – 59753	58897 – 60237
Data Span (yr)	2.1	2.7	4.0	2.4	3.7
Number of TOAs	34	79	144	88	37
Ref. epoch (MJD)	60000	59500	59500	59500	59500
Measured quantities					
RA (hh:mm:ss)	18:45:03.07708(4)	18:57:58.6789(2)	19:03:51.84526(5)	19:04:16.82283(4)	19:05:05.2578(13)
DEC(dd:mm:ss)	+02:01:49.363(6)	+06:42:30.656(2)	+08:39:17.1924(9)	+05:53:53.6127(9)	+06:49:49.33(5)
DM (cm ⁻³ pc)	56.653	21.5853(7)	166.451(2)	164.275(2)	187.668
ν (Hz)	232.0589209905(2)	283.20671122381(3)	216.39545569709(1)	203.77706071885(2)	36.41075526203(4)
$\dot{\nu}$ (10 ⁻¹⁶ Hz s ⁻¹)	-15.17(9)	-3.763(8)	-2.190(6)	-5.296(8)	-4.43(3)
PMRA (mas yr ⁻¹)	-	5.7(9)	-4.9(9)	-5.5(6)	-
PMDEC (mas yr ⁻¹)	-	1.6(10)	1.2(13)	-6.2(17)	-
px	-	-	-	4.5(17)	-
Residual (μ s)	2.082	2.506	4.193	3.328	75.868
EFAC	1.0	1.0	1.0	1.0	1.0
EQUAD	0.0	1.2	2.0	0.0	0.0
Reduced χ^2	1.22	1.23	1.19	1.24	0.75
Binary parameters					
Binary model	ELL1	ELL1	ELL1	ELL1	ELL1
P_b (d)	5.32570888(3)	6.734521817(6)	0.3126397707(3)	1.583625978(2)	1.381714792(2)
x (lt-s)	4.551805(2)	8.782903(3)	0.4050089(6)	1.4177437(9)	6.62159(5)
T_{asc} (MJD)	60002.988523(2)	59902.1721621(1)	59179.2317147(1)	59133.6085907(3)	59006.799191(2)
ϵ_1 (10 ⁻⁵)	0.72(18)	-0.53(5)	0.56(29)	-0.56(10)	1.9(20)
ϵ_2 (10 ⁻⁵)	1.55(8)	-0.39(3)	-0.10(36)	0.36(13)	-1.6(16)
Derived quantities					
l (deg)	34.012031(2)	39.6471272(9)	42.0453999(3)	39.6428450(3)	40.56309(3)
b (deg)	2.3462112(6)	1.6072138(5)	1.19956909(7)	-0.15604912(3)	0.093482(2)
D_{YMW} (kpc)	1.669	0.994	5.317	4.438	4.370
D_{NE2001} (kpc)	2.251	1.586	4.861	4.498	4.891
P (ms)	4.309250408179(3)	3.5309897695529(4)	4.6211691312030(2)	4.9073237020514(4)	27.46441244636(3)
\dot{P} (10 ⁻²¹ s s ⁻¹)	28.2(2)	4.69(1)	4.67(2)	12.75(2)	334(2)
τ (Gyr)	2.425	11.93	15.66	6.10	1.305
B_{surf} (10 ⁸ G)	3.526	1.30	1.48	2.53	30.64
e (10 ⁻⁵)	1.7(1)	0.66(4)	0.56(29)	0.67(11)	2.5(19)

Table A1. – continued –

Pulsar name	J1908+1036	J1911+1253	J1912+1416	J1916+0740	J1917+0615
GPPS number	gpps0114	gpps0181	gpps0169	gpps0166	gpps0460
MJD range	58989 – 60348	59271 – 60348	59256 – 60231	59263 – 60403	58713 – 60453
Data Span (yr)	3.7	3.0	2.7	3.1	4.8
Number of TOAs	131	90	44	118	39
Ref. epoch (MJD)	59500	59500	59500	59500	59500
Measured quantities					
RA (hh:mm:ss)	19:08:21.5212(2)	19:11:28.6990(2)	19:12:30.51373(5)	19:16:15.4327(7)	19:17:20.2887(2)
DEC(dd:mm:ss)	+10:36:35.368(4)	+12:53:17.414(5)	+14:16:23.674(2)	+07:40:41.175(11)	+06:15:29.192(3)
DM (cm ⁻³ pc)	10.915(3)	68.689(4)	66.665	219.86(2)	172.474
ν (Hz)	93.54365951465(1)	36.71246645742(1)	315.83188917471(4)	89.1292592477(1)	252.03522036226(7)
$\dot{\nu}$ (10 ⁻¹⁶ Hz s ⁻¹)	-1.376(5)	-0.583(4)	-8.039(13)	-1.59(4)	-13.42(3)
PMRA (mas yr ⁻¹)	-6.7(11)	-	-	-	-
PMDEC (mas yr ⁻¹)	-9.9(26)	-	-	-	-
Residual (μ s)	14.217	20.105	3.976	73.8	8.133
EFAC	1.6	0.74	1.0	0.93	1.0
EQUAD	2.4	0.0	0.0	0.0	0.0
Reduced χ^2	1.15	1.14	1.21	1.10	0.95
Binary parameters					
Binary model	ELL1	DD	ELL1	ELL1	ELL1
P_b (d)	3.964125977(2)	11.78905319(2)	0.2468944916(2)	14.8184145(3)	4.61843740(3)
x (lt-s)	11.388257(3)	20.437275(5)	0.329811(2)	7.315593(13)	3.55159(2)
T_{asc} (MJD)	59595.0312387(3)	-	59570.1674523(3)	59557.237288(6)	60000.264924(2)
e_1 (10 ⁻⁵)	-0.027(74)	-	-0.4(16)	2.07(61)	2.8(3)
e_2 (10 ⁻⁵)	-0.063(66)	-	-1.0(12)	0.30(34)	-3.6(11)
T_0 (MJD)	-	59664.9707(2)	-	-	-
e	-	0.0050267(5)	-	-	-
ω (deg)	-	250.479(6)	-	-	-
Derived quantities					
l (deg)	44.291270(2)	46.665604(1)	48.0101799(5)	42.594803(4)	41.461307(1)
b (deg)	1.1132798(3)	1.4864690(1)	1.90457045(8)	-1.971786(1)	-2.8694721(4)
D_{YMW} (kpc)	0.671	2.164	2.166	8.434	8.159
D_{NE2001} (kpc)	0.593	3.335	3.354	6.213	5.407
P (ms)	10.690195414509(2)	27.238703810866(9)	3.1662413906749(4)	11.21966017041(2)	3.967699429321(1)
\dot{P} (10 ⁻²¹ s s ⁻¹)	15.73(6)	43.3(3)	8.06(2)	20.0(5)	21.12(4)
τ (Gyr)	10.775	9.97	6.229	8.87	2.977
B_{surf} (10 ⁸ G)	4.14	10.99	1.617	4.79	2.930
e (10 ⁻⁵)	0.069(68)	-	1.1(12)	2.10(60)	4.6(9)

Table A1. – continued –

Pulsar name	J1917+1259	J1918+0621	J1924+1342	J1930+1403	J1932+2121
GPPS number	gpps0012	gpps0494	gpps0032	gpps0013	gpps0403
MJD range	58770 – 59985	58713 – 60344	58989 – 60518	58808-60408	59661 – 60254
Data Span (yr)	3.3	4.5	4.2	4.3	1.6
Number of TOAs	79	94	35	90	91
Ref. epoch (MJD)	59500	59500	59500	59500	59500
Measured quantities					
RA (hh:mm:ss)	19:17:21.3371(2)	19:18:00.6061(13)	19:24:16.5972(4)	19:30:17.62052(5)	19:32:21.2014(2)
DEC(dd:mm:ss)	+12:59:59.822(3)	+06:21:59.38(5)	+13:42:50.076(12)	+14:03:53.8022(7)	+21:21:06.786(2)
DM (cm ⁻³ pc)	117.017(4)	63.1179(3)	98.347	150.487(3)	192.101
ν (Hz)	177.38458504550(4)	475.3568747441(6)	174.7919902256(2)	311.58002361009(2)	70.20153107379(3)
$\dot{\nu}$ (10 ⁻¹⁶ Hz s ⁻¹)	-2.06(2)	-1.26(10)	-27.44(4)	-0.792(5)	-17.37(2)
Residual (μ s)	15.451	1.053	28.919	4.853	6.881
EFAC	1.0	1.0	1.0	1.0	1.0
EQUAD	0.0	0.0	0.0	1.4	0.0
Reduced χ^2	1.48	0.85	1.02	1.03	1.21
Binary parameters					
Binary model	ELL1	ELL1	ELL1	ELL1	ELL1
P_b (d)	3.201264482(5)	4.44919663(8)	3.5281740(2)	5.574928410(4)	0.0809057967(2)
x (lt-s)	5.896282(6)	2.73700(3)	1.60733(1)	5.180409(2)	0.1626938(15)
T_{asc} (MJD)	58890.9075574(7)	59899.843887(4)	59201.118335(4)	59216.6227321(3)	59688.9941818(3)
e_1 (10 ⁻⁵)	-4.75(16)	2.2(12)	-2.5(16)	0.35(4)	2.0(16)
e_2 (10 ⁻⁵)	-0.70(13)	-3.5(18)	-4.0(30)	1.88(4)	-2.0(14)
Derived quantities					
l (deg)	47.429743(1)	41.635129(5)	48.851147(3)	49.8554128(3)	56.4805218(9)
b (deg)	0.2701915(4)	-2.966894(2)	-0.8802052(2)	-1.99723150(8)	1.0786393(4)
D_{YMW} (kpc)	3.642	1.948	3.040	4.733	5.106
D_{NE2001} (kpc)	4.273	2.893	4.082	5.374	6.612
P (ms)	5.637468440357(1)	2.103682629053(3)	5.721085953135(6)	3.2094483735304(2)	14.244703565637(6)
\dot{P} (10 ⁻²¹ s s ⁻¹)	6.54(5)	0.56(5)	89.83(13)	0.815(5)	352.5(4)
τ (Gyr)	13.65	59.854	1.010	62.37	0.641
B_{surf} (10 ⁸ G)	1.94	0.346	7.254	0.51	22.676
e (10 ⁻⁵)	4.80(16)	4.2(16)	4.8(26)	1.91(4)	2.8(15)

Table A1. – *continued* –

Pulsar name	J1936+2035	J1938+2302	J1943+2206	J1946+0904	J1947+2011
	Observations				
GPPS number . . .	gpps0197	gpps0392	gpps0514	gpps0242	gpps0011
MJD range	58901 – 60257	59654 – 60392	59380 – 60540	59413 – 60545	58749 – 60165
Data Span (yr) . . .	3.7	2.0	3.2	3.1	3.9
Number of TOAs	57	277	166	35	125
Ref. epoch (MJD)	59500	60000	59500	60000	59500
	Measured quantities				
RA (hh:mm:ss) . . .	19:36:38.3072(7)	19:38:11.6306(4)	19:43:43.6485(3)	19:46:56.8707(2)	19:47:47.71374(9)
DEC (dd:mm:ss) . . .	+20:35:47.29(2)	+23:02:00.164(5)	+22:06:33.261(7)	+09:04:53.337(8)	+20:11:00.454(2)
DM (cm ⁻³ pc) . . .	198.861	303.365(8)	211.100	37.186	127.495(3)
ν (Hz)	30.36958214096(3)	18.953122076237(7)	213.59893407472(14)	38.801408988633(8)	122.285985983522(9)
$\dot{\nu}$ (10 ⁻¹⁶ Hz s ⁻¹)	-0.58(2)	-1.421(6)	-0.08(3)	-0.036(6)	-3.464(4)
Residual (μ s)	91.590	71.615	33.591	6.490	15.722
EFAC	1.0	1.0	1.0	0.7	1.0
EQUAD	0.0	0.0	0.0	0.0	5.0
Reduced χ^2	1.35	0.91	0.97	1.07	1.05
	Binary parameters				
Binary model	ELL1	DD	ELL1	DD	DD
P_b (d)	1.064143467(4)	33.9698770(2)	26.76246566(9)	6.037962681(10)	81.9689107(3)
x (lt-s)	5.64685(2)	54.670805(9)	23.79641(2)	7.135242(5)	37.803932(3)
T_{asc} (MJD)	59495.651756(1)	-	59003.294385(4)	-	-
e_1 (10 ⁻⁵)	-1.1(11)	-	0.77(6)	-	-
e_2 (10 ⁻⁵)	5.2(9)	-	-3.17(12)	-	-
T_0 (MJD)	-	59976.131(5)	-	59999.719(4)	59653.646(14)
e	-	0.0004038(3)	-	0.000344(3)	0.0001401(2)
ω (deg)	-	324.53(5)	-	335.59(22)	175.86(6)
	Derived quantities				
l (deg)	56.305424(6)	58.607434(2)	58.435492(2)	47.462644(2)	57.2431035(7)
b (deg)	-0.1625533(3)	0.7148274(7)	-0.85242037(4)	-7.9791543(4)	-2.63783970(3)
D_{YMW} (kpc) . . .	4.992	8.945	7.991	1.604	4.287
D_{NE2001} (kpc) . .	6.668	9.145	7.262	2.155	5.108
P (ms)	32.92768386995(3)	52.76175587207(2)	4.681671302958(3)	25.772259978831(5)	8.1775519243451(6)
\dot{P} (10 ⁻²¹ s s ⁻¹)	62.7(17)	395(2)	0.18(6)	2.4(4)	23.17(3)
τ (Gyr)	8.323	2.115	407.65	171.58	5.59
B_{surf} (10 ⁸ G) . . .	14.539	46.222	0.295	2.507	4.40
e (10 ⁻⁵)	5.3(9)	-	3.26(12)	-	-

Table A1. – *end* –

Pulsar name	J1952+2837	J2018+3518
GPPS number . . .	gpps0064	gpps0393
MJD range	58852 – 60624	59633 – 60045
Data Span (yr) . . .	4.9	1.1
Number of TOAs	126	83
Ref. epoch (MJD)	59500	60000
	Measured quantities	
RA (hh:mm:ss) . . .	19:52:49.65344(5)	20:18:48.149(7)
DEC (dd:mm:ss) . . .	+28:37:12.9120(9)	+35:18:45.85(5)
DM (cm ⁻³ pc) . . .	313.112(3)	266.994
ν (Hz)	55.490992750915(3)	31.932334792(1)
$\dot{\nu}$ (10 ⁻¹⁶ Hz s ⁻¹)	-6.5075(8)	-4.0(8)
Residual (μ s)	5.908	174.563
EFAC	1.4	1.0
EQUAD	0.6	0.0
Reduced χ^2	1.05	1.35
	Binary parameters	
Binary model	ELL1	ELL1
P_b (d)	0.8674946510(4)	3.3327156(1)
x (lt-s)	1.662420(3)	12.44297(5)
T_{asc} (MJD)	59415.77258787(8)	59969.165234(3)
e_1 (10 ⁻⁵)	-0.39(18)	3.4(7)
e_2 (10 ⁻⁵)	-0.21(16)	2.7(10)
	Derived quantities	
l (deg)	65.0916910(4)	73.69187(3)
b (deg)	0.6671998(2)	-0.37868(1)
D_{YMW} (kpc) . . .	10.474	7.077
D_{NE2001} (kpc) . .	9.722	8.435
P (ms)	18.0209426868383(8)	31.316219328(1)
\dot{P} (10 ⁻²¹ s s ⁻¹)	211.33(3)	388(80)
τ (Gyr)	1.35	1.279
B_{surf} (10 ⁸ G) . . .	19.75	35.283
e (10 ⁻⁵)	0.44(17)	4.3(8)

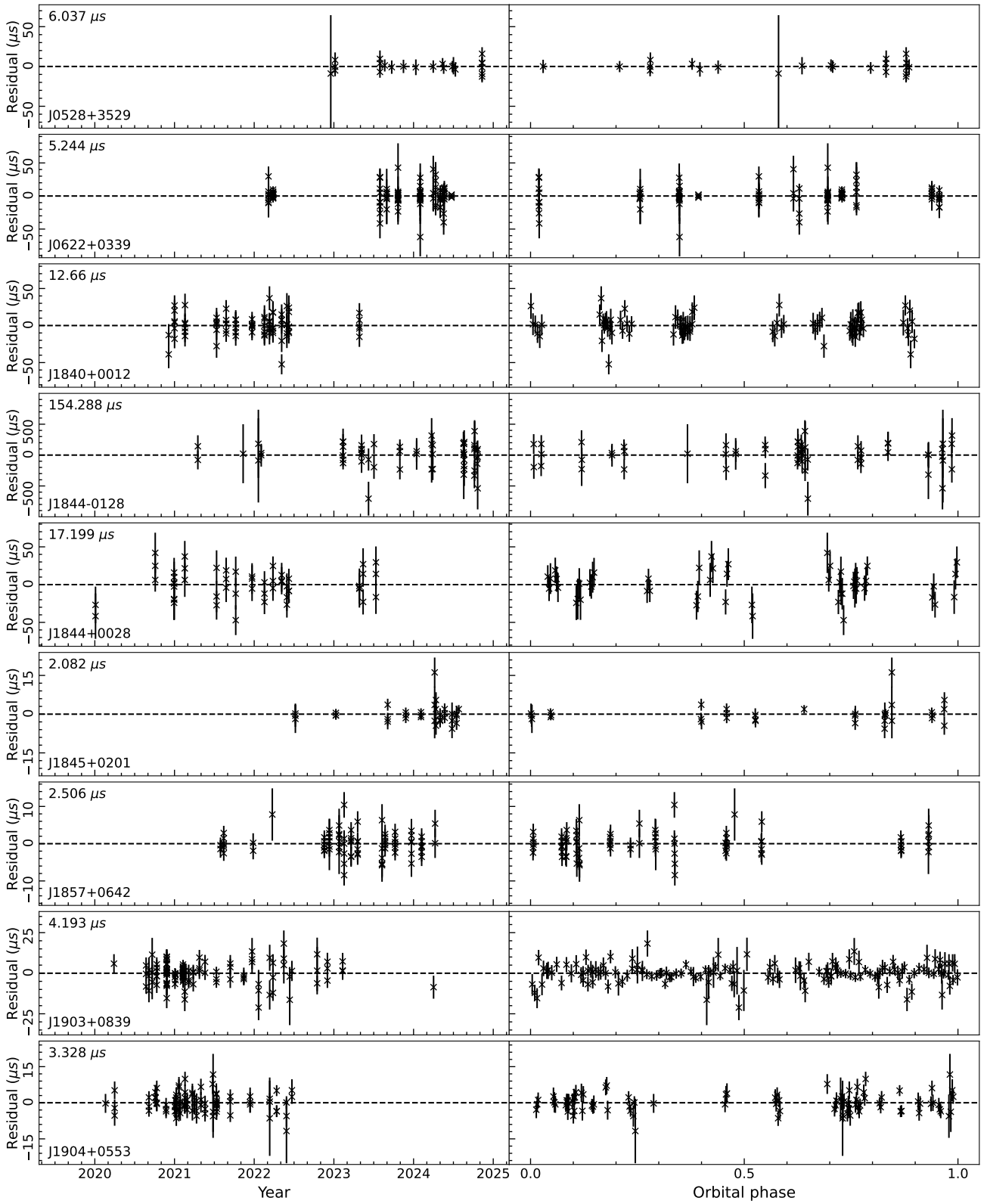


Figure A1. Timing residuals of 27 newly discovered binary pulsars by the FAST GPPS survey. *Left panels:* Residuals versus observation epochs. The weighted root-mean-square residual of each pulsar is indicated in the top right corner of the panel. *Right panels:* Residuals versus orbital phase. The orbital phases are referred to ascending node or periastron depending on the binary model of each pulsar.

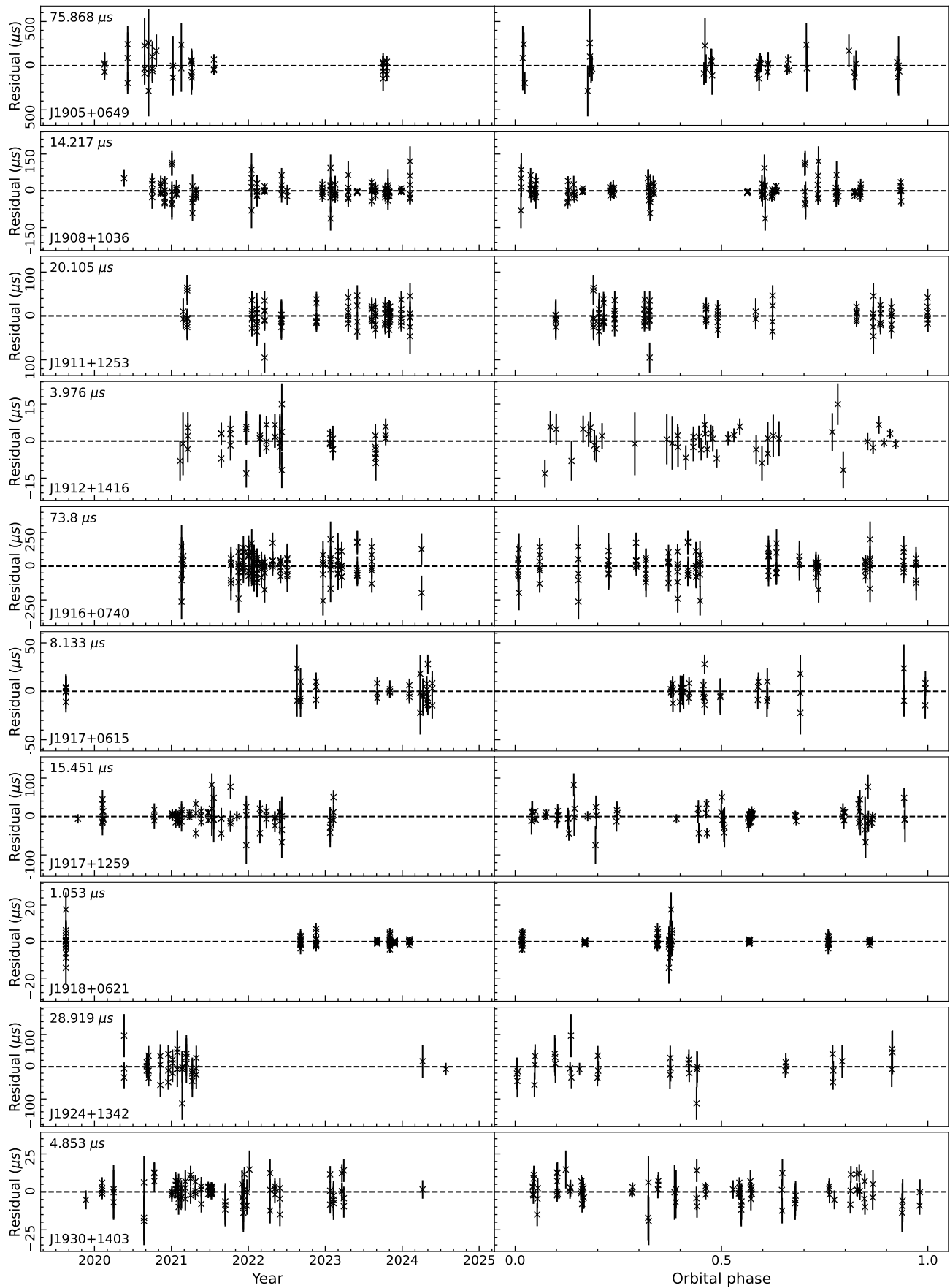


Figure A1. Continue—

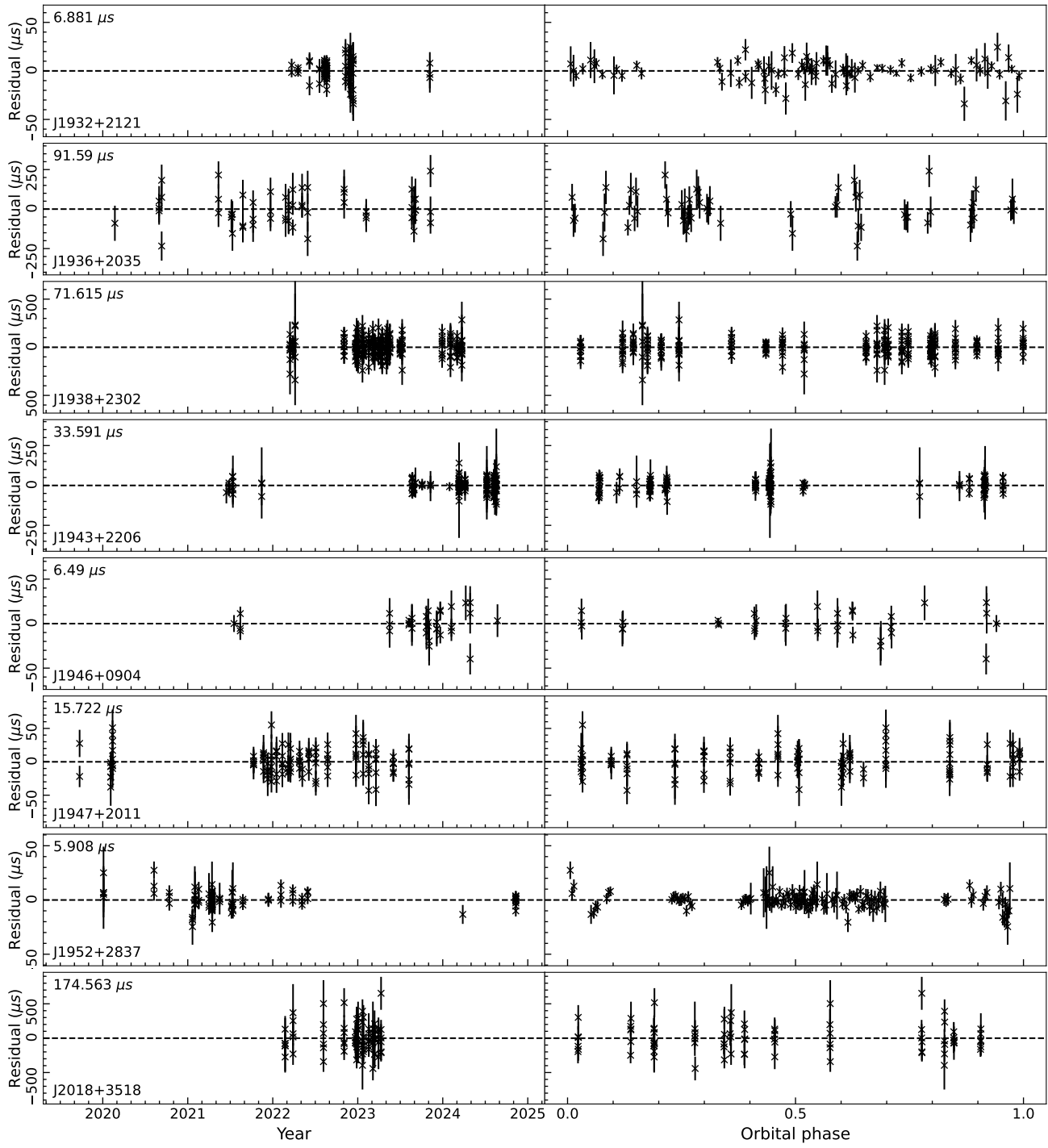


Figure A1. —End.

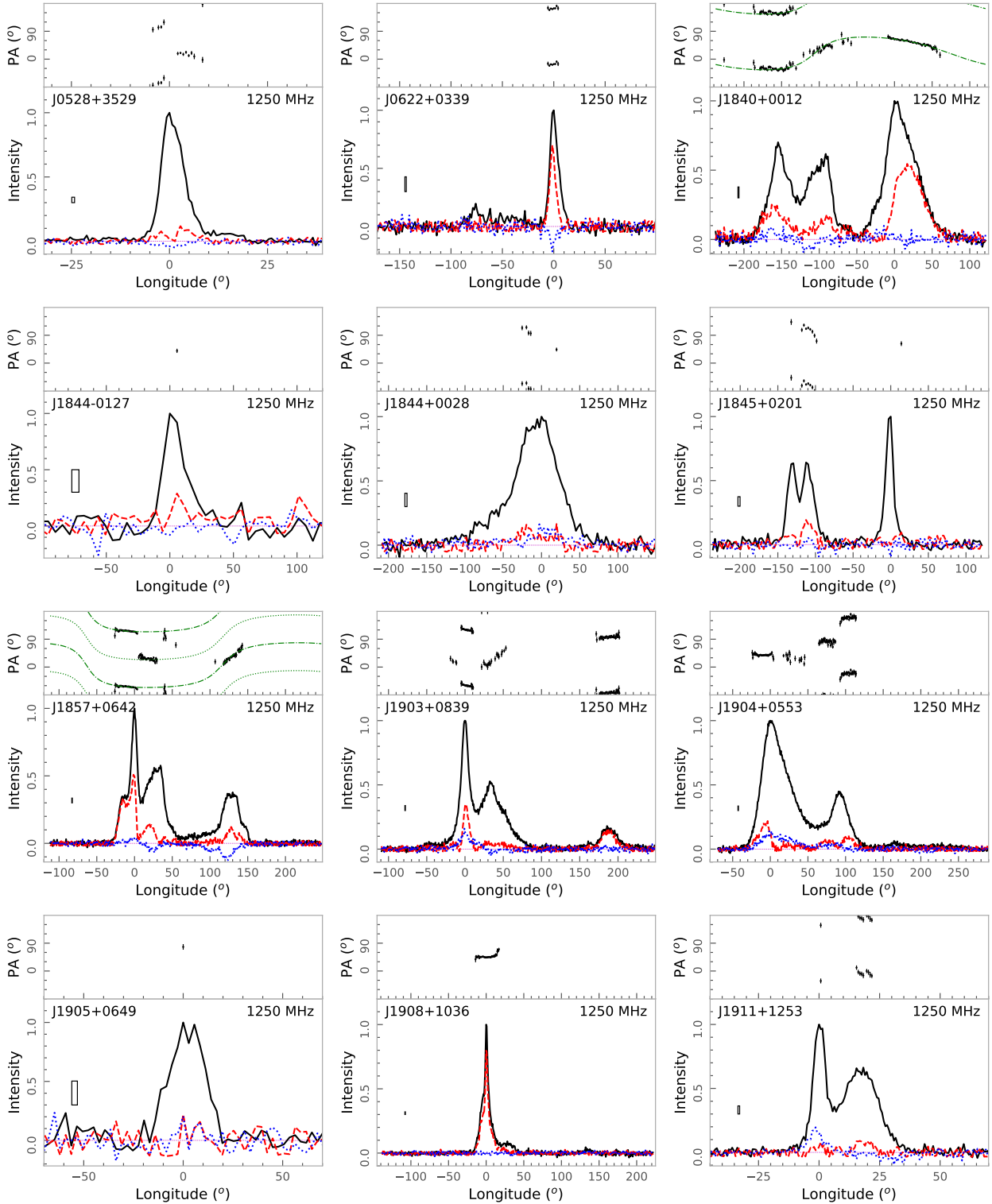


Figure A2. Integrated pulse profiles of 27 pulsars. The total intensity, linear and circular polarization are represented by solid, dashed and dotted lines in the bottom sub-panel. The left-hand circular polarization is defined to be positive. The bin size and 3σ are marked inside the sub-panel, here σ is the standard deviation of off-pulse bins. In the top panel, dots with error-bar are measurements of polarization position angles for linear polarization intensity exceeding 3σ line. The position angles are corrected to infinite frequency by discounting Faraday rotation. We tried to fit the polarization angle curves with the rotating vector model (Radhakrishnan & Cooke 1969) for 5 pulsars, PSRs J1840+0012, J1857+0642, J1916+0740, J1930+1403 and J1946+0904.

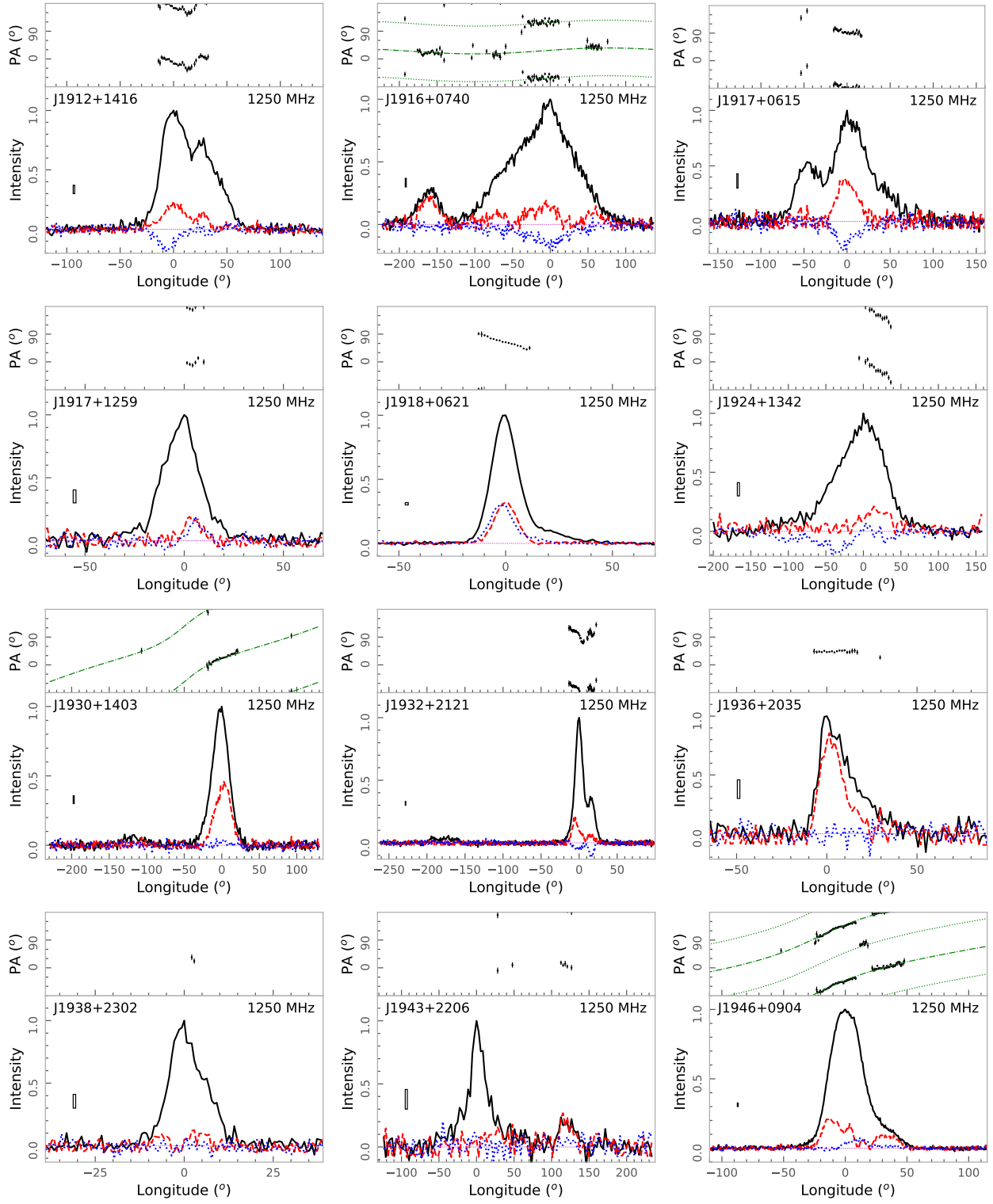


Figure A2. Continue—

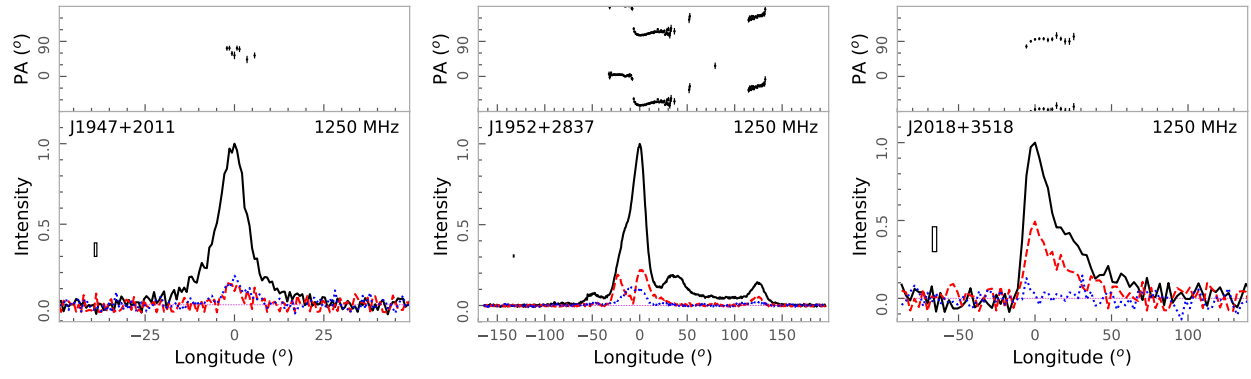


Figure A2. —End

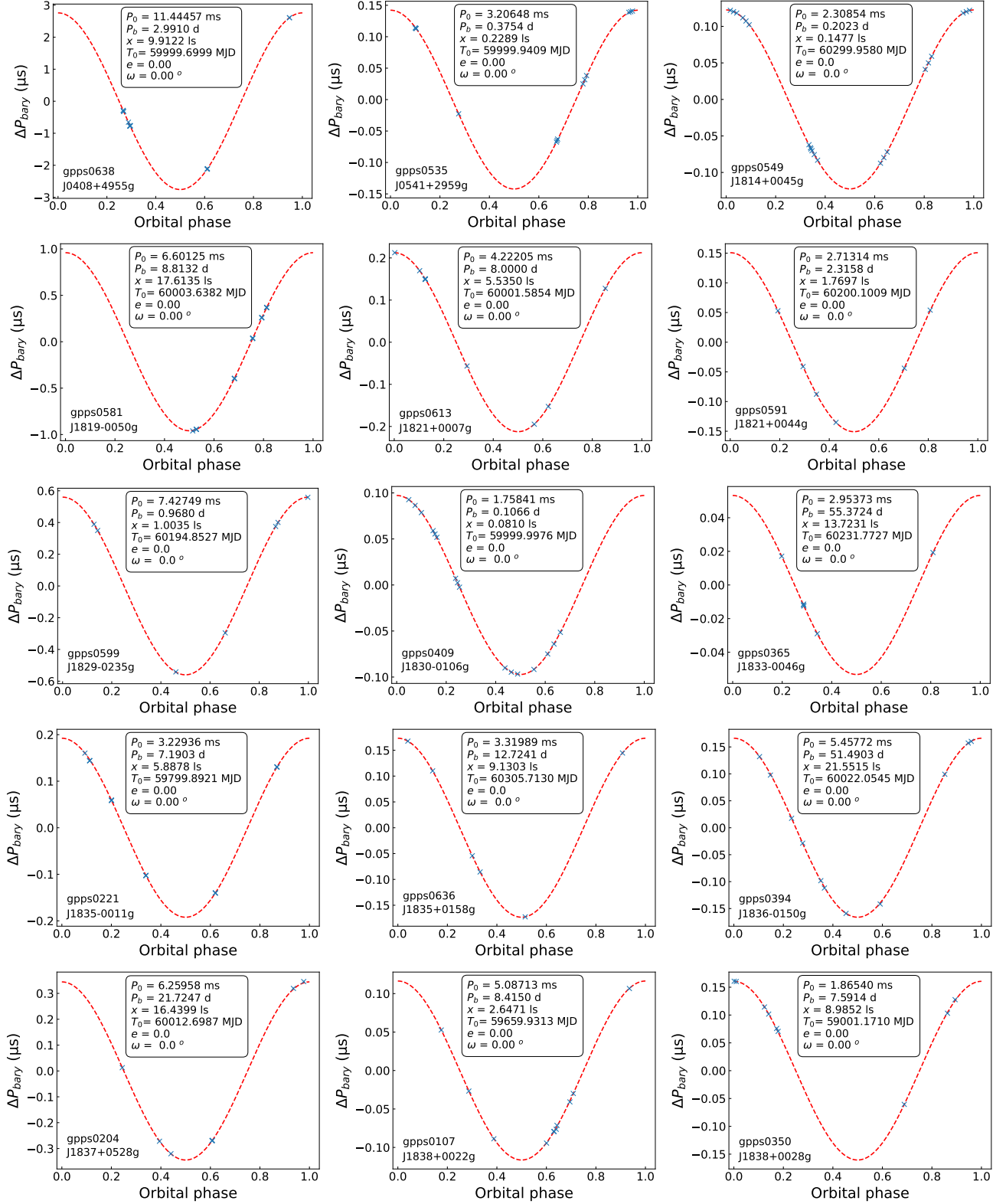


Figure A3. Variations of barycentric periods for 76 binary pulsars across the orbit phase. For each pulsar, the observed barycentric periods are marked by "x" after the average period P_0 is subtracted. The error-bars are marked but too small to see for most data. Dashed line is the best-fit by using the preliminary Keplerian model with orbital parameters (P_b , x , T_0 , e and ω) listed inside the panel. The orbital phase is referred to the periastron of the orbit.

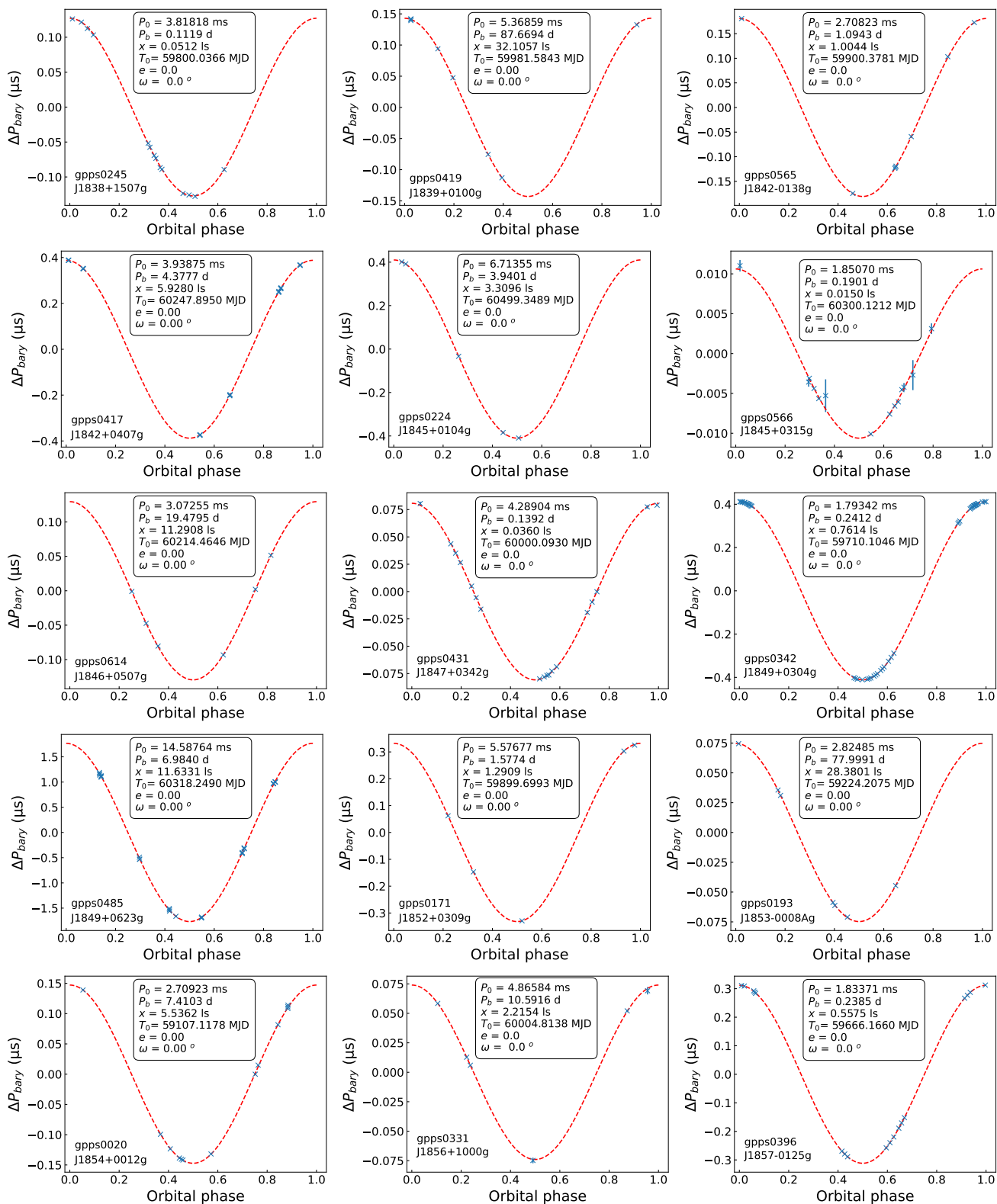


Figure A3. –continued–

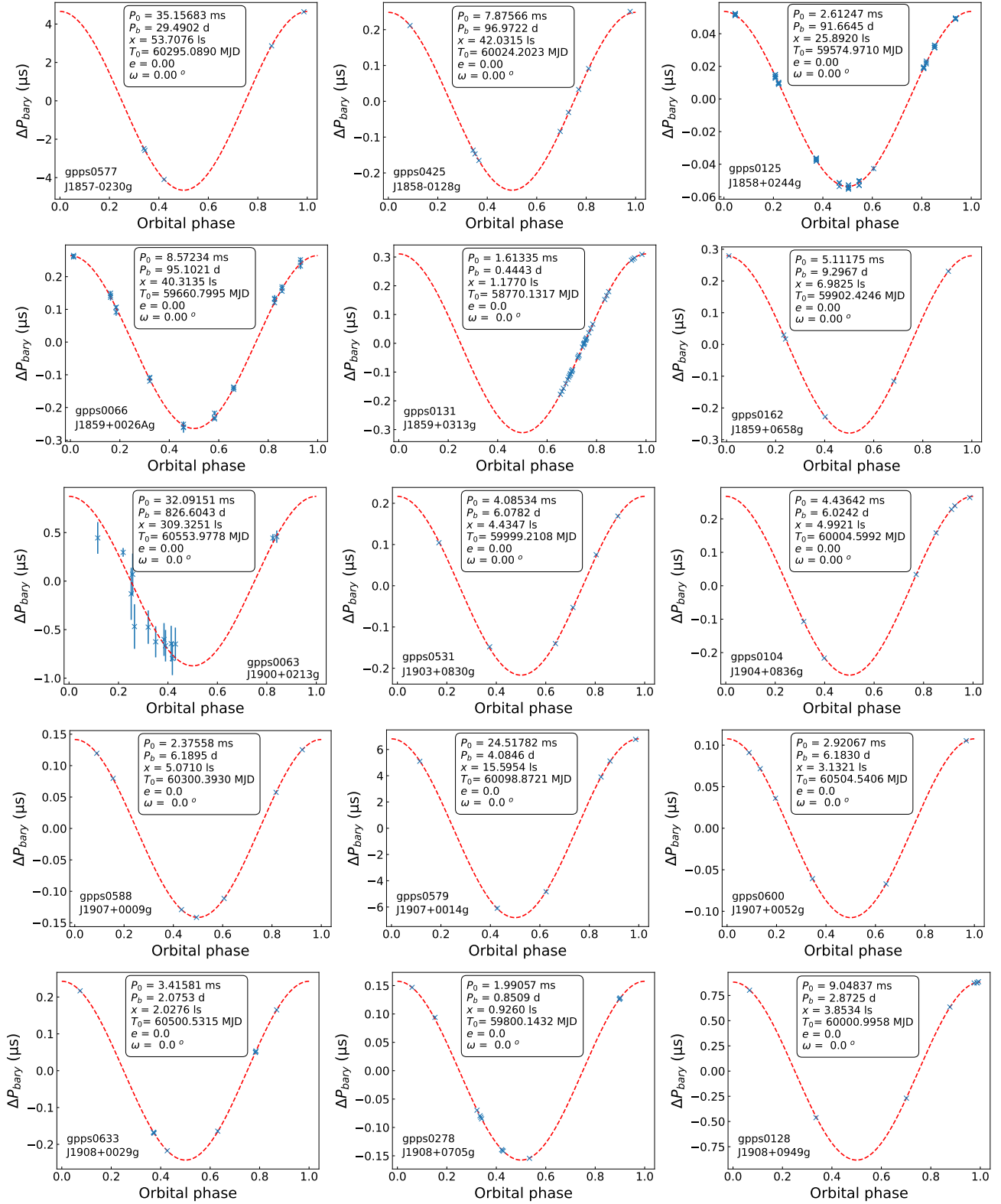


Figure A3. –continued–

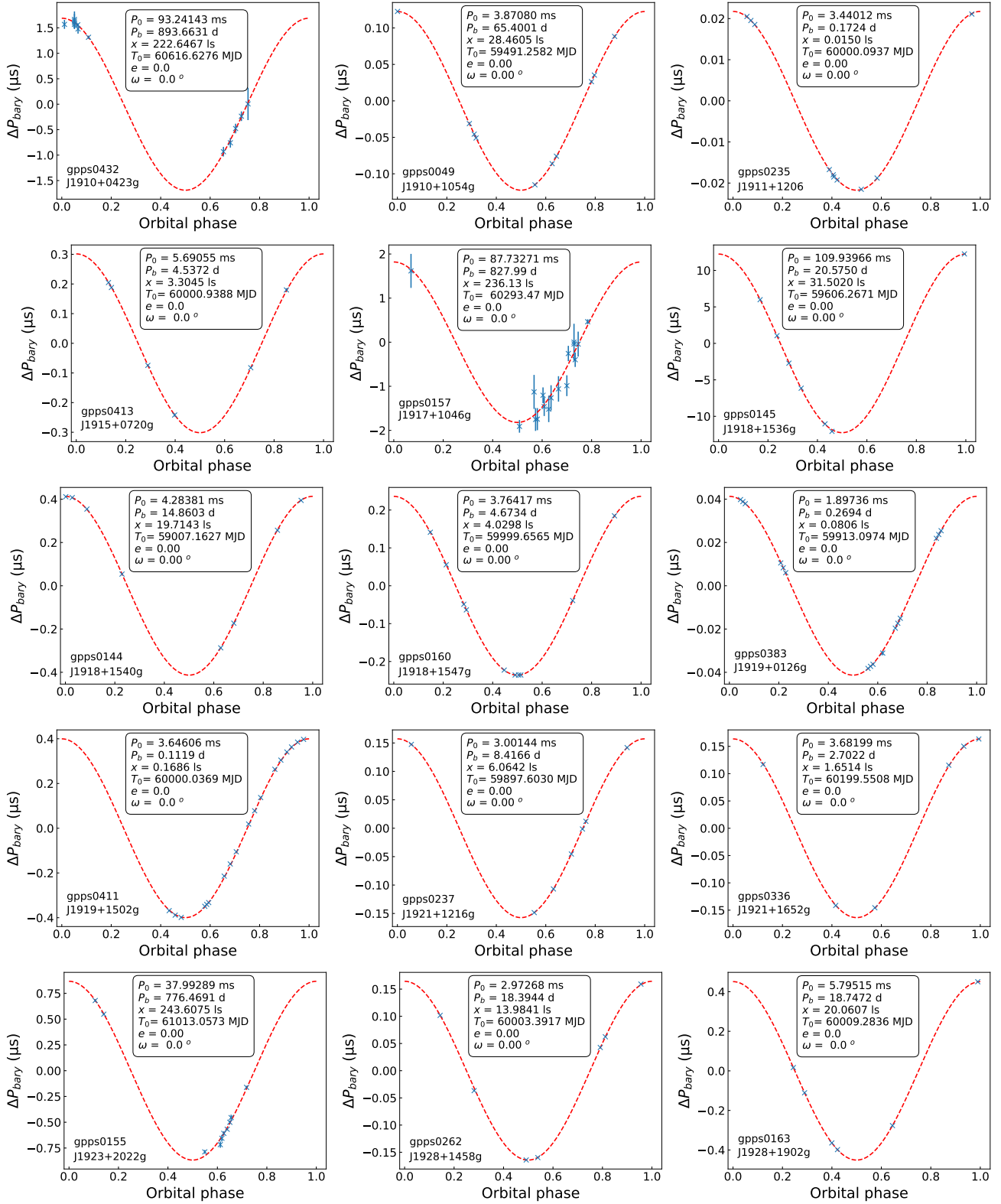


Figure A3. –continued–

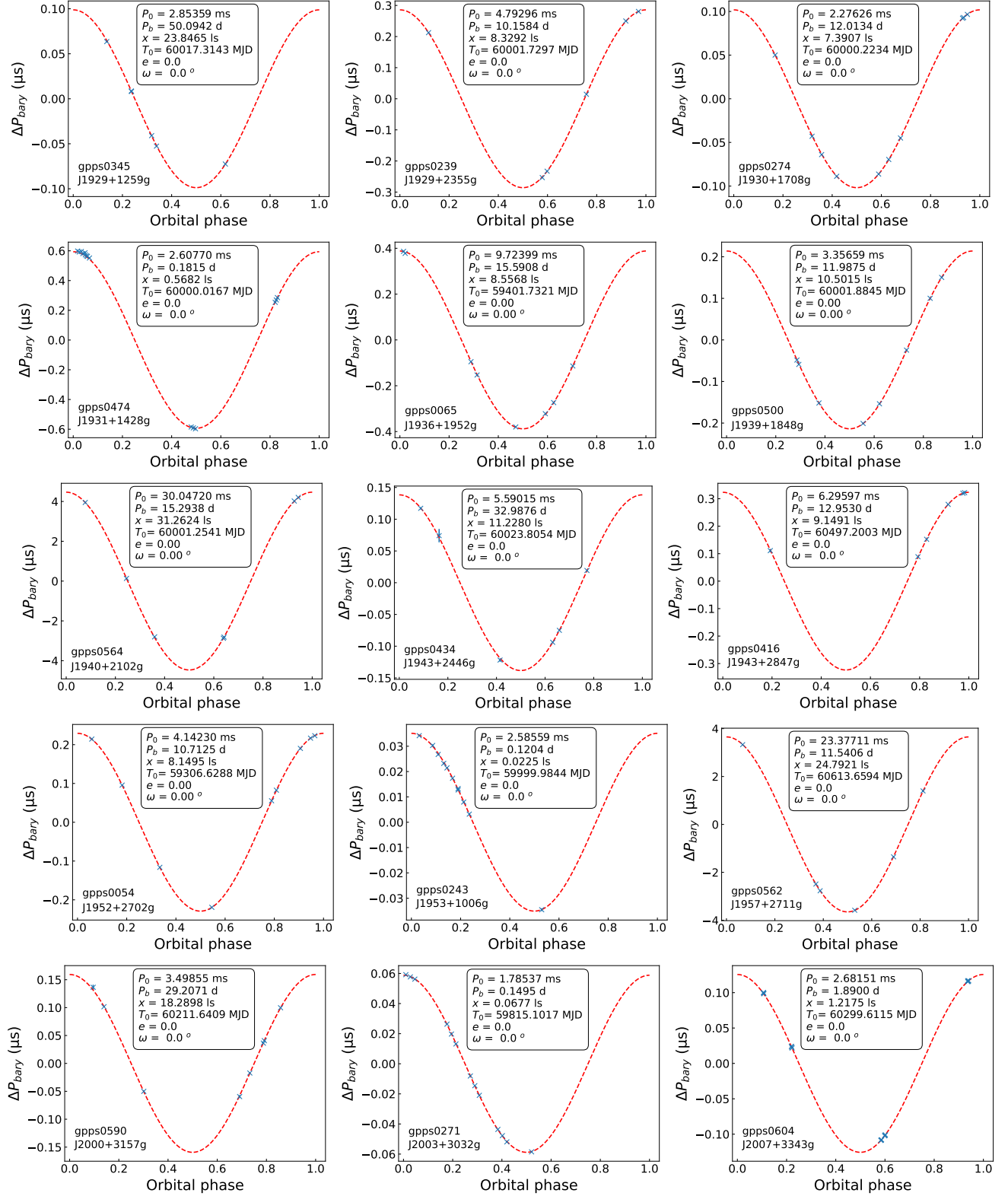
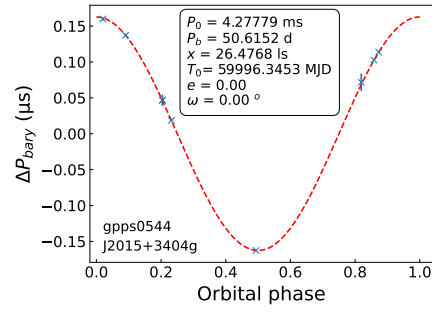


Figure A3. –continued–

**Figure A3.** –end.